[redacted]

ORNL
MASTER COPY

OAK RIDGE NATIONAL LABORATORY

operated by

UNION CARBIDE CORPORATION

for the

U. S. ATOMIC ENERGY COMMISSION

ORNL-TM-1200

2cy

16

FUELS AND MATERIALS DEVELOPMENT PROGRAM QUARTERLY PROGRESS REPORT FOR PERIOD ENDING JUNE 30, 1965

Classification Cancelled

[redacted]

By Authority Of AECM-2104 a2, B6a

By N Bray Date AUG 21 1974

CLASSIFICATION CANCELLED

David R. Hamrin 8/24/2011

ADD Signature Date

Single review of CCRP-declassified documents was authorized by DOE Office of Declassification memo of August 22, 1994.

[redacted]

Full release DRH

LEGAL NOTICE

This report was prepared as an account of Government sponsored work. Neither the United States, nor the Commission, nor any person acting on behalf of the Commission:

A. Makes any warranty or representation, expressed or implied, with respect to the accuracy, completeness, or usefulness of the information contained in this report, or that the use of any information, apparatus, method, or process disclosed in this report may not infringe privately owned rights; or

B. Assumes any liabilities with respect to the use of, or for damages resulting from the use of any information, apparatus, method, or process disclosed in this report.

As used in the above, "person acting on behalf of the Commission" includes any employee or contractor of the Commission, or employee of such contractor, to the extent that such employee or contractor of the Commission, or employee of such contractor prepares, disseminates, or provides access to, any information pursuant to his employment or contract with the Commission, or his employment with such contractor.

[redacted]

ORNL-TM-1200

Contract No. W-7405-eng-26

FUELS AND MATERIALS DEVELOPMENT PROGRAM QUARTERLY PROGRESS REPORT FOR PERIOD ENDING JUNE 30, 1965

Compiled by

P. Patriarca

SEPTEMBER 1965

OAK RIDGE NATIONAL LABORATORY
Oak Ridge, Tennessee
operated by
UNION CARBIDE CORPORATION
for the
U. S. ATOMIC ENERGY COMMISSION

[redacted]

[redacted]

FOREWORD

This is the fifth quarterly progress report describing work performed at the Oak Ridge National Laboratory for the Fuels and Materials Development Branch, Division of Reactor Development, U. S. Atomic Energy Commission. During FY-1966 two programs will be added: the work on controlled precipitation in nuclear ceramics will be reported by the Metals and Ceramics Division and that on fission-gas release from fuel materials during irradiation by the Reactor Chemistry Division. The specific programs covered are as follows:

Part I. Metals and Ceramics Division

Program Title	Person in Charge	Principal Investigator
Fuel Element Development	G. M. Adamson, Jr.	C. F. Leitten, Jr.
Mechanical Properties	D. A. Douglas, Jr.	J. R. Weir, Jr.
Nondestructive Test Development	D. A. Douglas, Jr.	R. W. McClung
Zirconium Metallurgy	C. J. McHargue	M. L. Picklesimer
Controlled Precipitation in Nuclear Ceramics	P. Patriarca	W. O. Harms

Part II. Reactor Chemistry Division

Fission-Gas Release from Fuel Materials During Irradiation	O. Sisman	R. M. Carroll
Physical Properties of Fuel Materials During Irradiation	O. Sisman	M. F. Osborne

[redacted]

[redacted]

TABLE OF CONTENTS

	Page
Summary	vii
Part I. Metals and Ceramics Division	
1. Fuel Element Development	3
Deposition of Uranium Dioxide by Hydroreduction of Uranium Hexafluoride	3
Direct Thermochemical Conversion of UCl_4 to UO_2	4
Deposition of Uranium Compounds by Lithium Reduction of UF_6	5
Deposition of Tungsten Alloys	5
Fabrication of Enriched UAl_3 Dispersion Fuel Plates	9
2. Mechanical Properties	13
Irradiation Embrittlement of Low-Boron Type 304 Stainless Steel	13
Irradiation Embrittlement of Stainless Steel at Very High Temperatures	17
Ductility of Irradiated 18-8 Type Stainless Steels Containing Titanium	21
3. Nondestructive Test Development	24
Electromagnetic Test Methods	24
Ultrasonic Test Methods	27
Nonbond Studies	27
Tubing Inspection	28
Penetrating Radiation Methods	29
Gamma Scintillation Gaging	29
X-Ray Projection Microscopy	29
Inspection Development of Problem Materials	30
4. Zirconium Metallurgy	31
Effect of Preferred Orientation and Stress on the Directional Precipitation of Hydrides in Zircaloy-2	31
Hydride and Basal Pole Figures in Zircaloy-2 by Quantitative Metallography	35
Tube Testing Apparatus	35
Optical Properties of Zirconium Alloys	36

[redacted]

[redacted]

Oxide Film Studies 39

Preparation of Single Crystals of Zirconium and Zirconium Alloys 40

Electrical-Discharge Machining 40

Zone Refining of Zirconium 41

Properties of High-Purity Zirconium 41

Recrystallization 41

Oxidation 42

5. Controlled Precipitation in Nuclear Ceramics 44

Effect of Precipitation on the Properties of Nonfissile Ceramics 44

Part II. Reactor Chemistry Division

6. Fission-Gas Release from Fuel Materials During Irradiation 51

Experimental Method 51

Release of Fission Gas 55

Recoil Escape 56

Temperature-Dependent Release 57

Defect-Trap Model 59

Theoretical Considerations 60

Grain Boundary Effect 61

Dynamic Experiments 62

Experimental Method 63

7. Physical Properties of Fuel Materials During Irradiation 65

[redacted]

[redacted]

SUMMARY

1. Fuel Element Development

We have continued the development of both fuel and cladding materials by thermochemical deposition techniques. During this period, the fuel work was concentrated on the synthesis of UO_2 powders. The deposition apparatus was modified for production of powders. A brown powder with an oxygen-to-uranium ratio of 2.074 was produced. Hydrogen firing this powder yielded an oxygen-to-uranium ratio of 2.001. Equipment was installed for the direct conversion of UCl_4 to UO_2 and for the deposition of uranium compounds by lithium reduction of UF_6.

The cladding studies concentrated on the deposition of tungsten-rhenium alloys. The previously reported problems of axial variation in composition and deposition rates have been greatly minimized by the use of a short moving hot zone instead of a fixed furnace. In a 6-in. deposit, the variation in rhenium content has been limited to 19 to 27% with a 25% Re charge; the metal recoveries were 100%. As yet smooth surfaces have not been achieved.

Experiments with binary mixtures of WF_6 with small amounts of either BCl_3, VF_5, or MoF_6 have demonstrated the feasibility of adding small amounts of alloying additions to tungsten by vapor deposition. Problems of nonuniformity have not been solved. The addition of VF_5 has produced some breaking up of the large columnar tungsten grains.

As an alternate fuel for research reactors, UAl_3 has been produced by powder-metallurgy techniques. A more nearly stoichiometric product was obtained than had been possible by the previous arc-melting process. Satisfactory fuel plates were fabricated from the UAl_3 using conventional hot-roll bonding techniques. These plates will be irradiated in the ORR.

[redacted]

2. Mechanical Properties

Recent investigations have emphasized the elevated-temperature radiation-induced ductility problem in type 304 stainless steel. Our objectives in this part of the program have been to determine the mechanism for the damage and to attempt to alleviate the problem by metallurgical treatment of the material prior to irradiation.

Several laboratory heats of type 304 stainless steel were produced by electron-beam melting to reduce the boron content in the alloy to very low values. Reducing the boron content to very low values was found to be only a partial solution to the problem. This is because at normal fast-to-thermal neutron flux ratios one finds that the helium generated from fast (n,α) reactions becomes significant compared to the helium generated from the thermal neutron ^{10}B (n,α) reactions at a boron content of about 1 ppm.

The effects of irradiation on stainless steel at temperatures up to 900°C show that irradiation at this temperature produces greater damage than irradiation at temperatures below 800°C. This is believed to be associated with the fact that carbides are soluble at the high temperature. It is also shown that the quantity and distribution of carbides are very important factors influencing the magnitude of the damage.

The assumption that boron is the primary cause for the high-temperature radiation-induced embrittlement leads to investigation of ways to influence the distribution of boron in the material. We have chosen a titanium addition as a possible technique to "tie up" the boron as a compound in these steels. The results of these studies show a pronounced improvement in the postirradiation ductility of type 304 stainless steel with 0.2% Ti.

[redacted]

3. Nondestructive Test Development

We are developing new techniques and equipment for the nondestructive evaluation of materials and components. The major emphasis has been on eddy-current, ultrasonic, and penetrating-radiation methods.

The mathematical approach using a computer to analyze variations in electromagnetic field parameters has been applied to the problem of a long coil above a conducting plane. Calculations have been made for the phase and amplitude of the vector potential and density of the current for this case.

The ultrasonic test developments have included techniques for nonbond evaluation in hot cells on tubular fuel elements. We are continuing to develop calibration curves and techniques for electro-discharge machining of reference notches in tubing. We have developed techniques for ultrasonically inspecting tapered tubing.

We have begun preliminary calibration and modification of our gamma-attenuation fuel rod scanner. Our assembly of an x-ray projection microscope from electron-optical components is showing good progress.

The work on problem materials has included tungsten-, tantalum-, titanium-, and niobium-base alloys.

4. Zirconium Metallurgy

A study of the effects of stress level, stress direction, hydrogen content, and preferred orientation of the matrix on the orientation of hydrides precipitated under elastic stress has been completed. A report presenting the data in detail is in preparation. The previously reported conclusion that the hydrides are oriented perpendicular to the tensile stress during precipitation only when that stress is along a basal pole concentration in the matrix has been confirmed. There may be preferential sites for hydride precipitation which are occupied at the lower hydrogen contents, forcing less favorable sites to be occupied when the hydrogen content is increased.

[redacted]

The tube testing apparatus has been completed and the programming and control instrumentation debugged. Full-scale testing will proceed as soon as the internal pressure and volume measuring systems have been checked.

Some of the optical properties of a single-crystal sphere of zirconium were measured in a polarized light microscope as functions of wavelength of the incident light and crystallographic plane. The data are of considerable theoretical interest but are of immediate practical utility in determining from a single-surface examination the orientation in space of the basal pole of any grain of zirconium whose basal plane is tilted more than about 10 deg to the surface of the specimen.

Fast (>1 Mev) neutron irradiation to 10^{19} neutrons/cm^2 had negligible effect on the rate of dissolution of anodically formed oxide films on zirconium. The dissolution itself was found to increase greatly the optical absorption of the oxide film, indicating a change in the defect structure of the oxide. Attempts to strip the base metal from the partially dissolved oxide films for transmission spectrophotometer measurements failed because the base metal was severely attacked through the oxide film, again indicating appreciable changes in the structure of the oxide film.

The carbon and oxygen contamination in zone-refined zirconium has been reduced by modifying the baking and operational procedures of our zone refiner. Carbon pickup is less than 2 ppm per pass, and oxygen contents can be kept below 20 ppm during four passes.

Recrystallization starts in less than 10 hr at 175°C in zone-refined zirconium and is completed in less than 100 hr at that temperature, yielding a grain size of about 10 μ. The recrystallization appears to occur by the conventional nucleation and growth process.

The dissolution rates of anodically formed oxide films on single crystals of zirconium are being determined by direct visual observation and comparison to color standards. The dissolution rate at 580°C appeared to decrease with time.

5. Controlled Precipitation in Nuclear Ceramics

A program was initiated to assess the role of controlled, homogeneous precipitation of second phases on improving the fission-gas release, swelling, and mechanical characteristics of both fissile and nonfissile nuclear ceramic materials. Preliminary work on preparation and characterization of titanium-doped alumina single crystals is reported.

6. Fission-Gas Release from Fuel Materials During Irradiation

The mechanism of the release of fission gas from uranium dioxide during irradiation is being studied by continuously monitoring the release from carefully characterized specimens irradiated under controlled conditions. The temperature and flux are independently controlled up to 1400 °C and 10^{14} neutrons cm^{-2} sec^{-1}, respectively. The fission gas is carried out of the reactor by a sweep of purified helium and analyzed with a gamma spectrometer.

The release rate of fission gas was observed to be temperature dependent above about 600 °C and independent of temperature at lower temperatures. According to classical theory this would correspond to diffusion-controlled release in the temperature-activated region and recoil release at the lower temperatures. We find that the low-temperature release is by knockout rather than direct recoil, and the temperature-activated release cannot be explained by a diffusion mechanism. A defect-trap mechanism is proposed, and it appears to satisfy all of the experimental observations.

A mathematical model for the defect-trap mechanism of fission-gas release is being developed; and in order to fully evaluate the mathematical model, the experiment has been modified to operate in a dynamic mode as well as the steady-state mode. First experiments with the dynamic experiments have been very encouraging and have qualitatively further substantiated the defect-trap model.

[redacted]

7. Physical Properties of Fuel Materials During Irradiation

Plans are being made for the first in-reactor physical property experiment. In this experiment we will study thermal conductivity on a single crystal of uranium dioxide at temperatures up to 1400°C.

[redacted]

[redacted]

PART I

METALS AND CERAMICS DIVISION

[redacted]

[redacted]

[redacted]

1. FUEL ELEMENT DEVELOPMENT

G. M. Adamson, Jr.

The Fuel Element Development Program continues to be directed toward development of new or improved fabrication techniques for both fuels and cladding materials. At present, we are emphasizing thermochemical deposition both for conversion of uranium halides to uranium dioxide and as a means for fabricating refractory metal cladding materials such as tungsten or tungsten alloys.

We have demonstrated that uranium hexafluoride may be directly converted to uranium dioxide by a high-temperature hydroreduction reaction. The product may be obtained as a solid approaching theoretical density, a dendritic needle-like deposit, or a submicron size powder. Investigations are under way to determine the feasibility of similar reactions for the conversion of uranium tetrafluoride to uranium dioxide. In addition the conversion of uranium hexafluoride to uranium carbide is being investigated by vapor-phase lithium reduction.

Refractory metal cladding materials have been fabricated by the coreduction of tungsten and rhenium hexafluoride by hydrogen to produce tungsten-rhenium alloys. We are continuing investigating means of producing uniform homogeneous deposits by a moving hot-zone technique.

Improvements in the performance characteristics of aluminum-base dispersion fuel elements are being sought through studies of fabrication behavior.

Deposition of Uranium Dioxide by Hydroreduction of Uranium Hexafluoride

R. L. Heestand C. F. Leitten, Jr.

Studies of the effects of gas feed ratios on stoichiometry of solid uranium dioxide deposits have been suspended in the interest of further studies in uranium dioxide powder synthesis. Experiments conducted previously[1] for powder fabrication were reviewed and similar conditions

[1]R. L. Heestand and C. F. Leitten, Jr., Fuels and Materials Development Program Quart. Progr. Rept. June 30, 1964, ORNL-TM-920, pp. 3–6.

applied to several experiments. Since many modifications had been made in the apparatus for solid UO_2 deposition, it was impossible to readily duplicate the previous powder runs particularly since difficulties had been encountered at that time in accurately metering UF_6 and steam through the duration of an experiment.

Previously powder runs had given a black product which by chemical analysis was found to be hyperstoichiometric with oxygen being as high as $UO_{2.312}$. X-ray analyses of these deposits indicated only UO_2 to be present with less than 5% impurities.

When the experiments were repeated, a brown powder was obtained over wide variations in conditions. The material was again identified by x-ray analysis as uranium dioxide with chemical analysis giving an oxygen-to-uranium ratio of 2.074. Subsequently the powder was hydrogen fired at 1000°C for 3 hr which gave an adjusted oxygen-to-uranium ratio of 2.001. Samples have been submitted to determine fluorine content of the powder.

Experiments are continuing to optimize conditions for powder production and minimize fluorine content.

Direct Thermochemical Conversion of UCl_4 to UO_2

F. H. Patterson W. C. Robinson, Jr. C. F. Leitten, Jr.

As previously reported,[2] thermodynamic calculations were made to investigate the feasibility of direct conversion of UCl_4 to UO_2 by the chemical vapor deposition process. Actual observations[3] have indicated that this reaction will proceed.

Experimental facilities necessary for this investigation have been completed. Feasibility studies will proceed as soon as time permits.

---

[2]F. H. Patterson, W. C. Robinson, and C. F. Leitten, Jr., Fuels and Materials Development Program Quart. Progr. Rept. March 31, 1965, ORNL-TM-1100, pp, 3-4.

[3]Personal communication to W. C. Robinson, Jr. from T. A. Gens, Chemical Technology Division, December 1964.

Deposition of Uranium Compounds by Lithium Reduction of UF_6

W. C. Robinson, Jr. C. F. Leitten, Jr.

The experimental facilities necessary for the investigation have been constructed. The facilities have two metal-to-metal seals which must be vacuum tight at 600 to 800°C. Difficulties have been encountered with one of these seals and the apparatus has been modified several times in an effort to stop the leak. This problem should be solved and the initial experiments performed within the next report period.

Deposition of Tungsten Alloys

J. I. Federer C. F. Leitten, Jr.

Deposition of tungsten-rhenium alloys by hydrogen reduction of WF_6 and ReF_6 has continued. Since deposition on the inner wall of tubular mandrels in a stationary hot zone results in axial variations in composition and deposition rates,[4] a moving hot-zone technique was attempted.[5] In the initial experiments an 8-in.-long furnace was moved in intervals. This moving hot zone maintained a relatively high rhenium content throughout a greater length of deposit than had been possible previously. Subsequently, the furnace was replaced with a 1-in.-long induction coil. A mechanical device moves the deposition tube through the induction coil at a constant rate. Before entering the deposition zone the reactant gases are preheated to about 300°C. Conditions and results of these experiments are shown in Table 1.1. In these experiments the total feed rate of WF_6 and ReF_6 was less than in previous moving hot-zone experiments, and metal recoveries of 100% were obtained. The axial variations in rhenium content shown in Table 1.1 can only be evaluated in the center sections due to the end effects from temperature gradients

[4] J. I. Federer and C. F. Leitten, Jr., Fuels and Materials Development Program Quart. Progr. Rept. Dec. 31, 1964, ORNL-TM-1000, pp. 4–10.

[5] J. I. Federer and C. F. Leitten, Jr., Fuels and Materials Development Program Quart. Progr. Rept. Mar. 31, 1965, ORNL-TM-1100, pp. 7–9.

[redacted]

Table 1.1. Conditions[a] and Results of Tungsten-Rhenium Deposition Experiments Using a Moving Hot Zone

Alloy Designation	Gas Composition, cm^3/min			Hot-Zone Movement (in./hr)	Distance from Inlet (in.)	Rhenium Content (%)
	H_2	WF_6	ReF_6			
WRe-30	250	15	5	0.75	1	
					2	28
					3	22
					4	19
					5	
					6	
WRe-31	500	30	10	0.75	1	13
					2	23
					3	29
					4	26
					5	12
					6	
WRe-32	500	30	10	0.75	1	11
					2	22
					3	27
					4	24
					5	22
					6	19
WRe-33	500	30	10	1.50	1	19
					2	27
					3	27
					4	24
					5	26
					6	21

[a]Temperature: 750°C
Pressure: 10 torr
Recovery: 100%

[redacted]

which give a lower rhenium content on both the leading and trailing ends of the deposit. Nevertheless, the high metal recoveries and the correlation between gas composition (25% ReF_6 excluding hydrogen) and the high rhenium content of the deposits (27 to 29%) is encouraging.

Deposits prepared in this manner have circumferential ridges of varied height, width, and spacing consisting of growth cones or nodules. The bulk deposits have a columnar grain structure and a smooth surface texture between the ridges. The deposition rate on the ridges is about double the rate on adjacent bulk material. For example, in a nominally 20-mil-thick deposit the ridges are about 20 mils high, 20 to 40 mils wide, and spaced 1/16 to 1/4 in. apart. The ridges are attributed to nonuniform heating in the stainless steel deposition tube. Under similar deposition conditions, decreasing the pitch of the coil results in a decrease in the height and spacing of the ridges. Increasing the rate of hot-zone movement has a similar effect. Various combinations of temperature (700 to 800°C), pressure (3 to 10 torr), and gas preheating (25 to 300°C) have substantially no effect on the ridges. Consequently, a susceptor is being employed to receive direct heating from the induction coil. The susceptor, in turn, radiates directly to the deposition tube which results in an even temperature distribution. Experiments are now being conducted to evaluate this arrangement.

The deposition of fine-grained, rather than the usual columnar-grained tungsten has been attributed to unintentional contamination with vanadium and molybdenum.[6] In continuing deposition experiments small amounts of certain alloying elements are being added to tungsten by coreduction of the mixed fluorides. The objective of these experiments is to study methods for adding known quantities of the elements to tungsten.

In early experiments coreduction of a mixture containing about 0.06% VF_5 in WF_6 at 600, 700, and 800°C resulted in vanadium contents

---

[6]J. I. Federer and C. F. Leitten, Jr., Fuels and Materials Development Program Quart. Progr. Rept. Mar. 31, 1965, ORNL-TM-1100, pp. 9–11.

ranging from < 10 to 75 ppm (ref. 6) but with no effect on structure. These codeposition experiments have continued with higher concentrations of VF_5 and also with boron and molybdenum by using binary mixtures of the halides under the following conditions:

Temperature	600, 700, 800°C
Pressure	10 torr
H_2	1000 cm^3/min
WF_6 + 0.5% BCl_3	50 cm^3/min
WF_6 + 2.1% VF_5	50 cm^3/min
WF_6 + 0.5% MoF_6	50 cm^3/min
Deposition mandrel	7/8-in. OD × 3/8-in. ID × 12-in.-long copper tube (internal deposit)

The WF_6 + BCl_3 mixture was metered at 38°C where the vapor pressures of the two constituents are equal. The other two mixtures were metered at the boiling points of VF_5 (50°C) and MoF_6 (35°C).

Suppression of tungsten deposition occurred with each mixture. For example, no deposit was obtained at 600°C with the WF_6 + 2.1% VF_5 mixture and only 50% recovery was obtained at 600°C with the WF_6 + 0.5% BCl_3 mixture. Metal recoveries, however, increased with increasing deposition temperature. Samples for chemical analysis and metallographic examination were taken at 2-in. intervals along the length of the deposits. Boron additions, if any, were less than the limit of detection of 50 ppm. Vanadium contents ranged from 880 to 1130 ppm, and molybdenum < 20 to 1000 ppm with the highest concentration of additives occurring at the gas inlet end of the deposit.

The microstructures of samples prepared with fluoride mixtures containing BCl_3 and MoF_6 were columnar with a very fine precipitate at the grain boundaries and, to a lesser extent, within the grains. No other characteristic microstructural features were observed. Several of the samples prepared with a mixture containing VF_5 had regions of VF_3 included in the microstructure. The vanadium content of these samples was not included in the range of values mentioned previously. The microstructure of two samples from two different deposits prepared at 800°C was unlike any previously observed, being neither columnar nor equiaxed.

The grains were elongated in the growth direction but did not extend completely through the deposits. The columnar structure was apparently disrupted by the frequent nucleation of new grains as deposition proceeded.

These experiments have demonstrated the feasibility of adding small amounts of alloying additions to tungsten by vapor deposition, but the process is subject to the nonuniformity problem observed in the deposition of tungsten-rhenium alloys.[7] Such additions do show promise of being grain refiners. Several methods are being considered to minimize this problem, including deposition on a male mandrel contained in a mixing chamber and the use of a moving hot zone.

Fabrication of Enriched UAl_3 Dispersion Fuel Plates

W. J. Werner J. H. Erwin M. M. Martin
C. F. Leitten, Jr.

A number of problems are anticipated with fuels for very high performance aluminum-water research reactors. The need for incorporating burnable poisons in fuel plates precludes the use of alloy fuels since large and erratic boron losses have been experienced during melting. The metastable nature of the oxide dispersions in combination with large gas releases that could accompany the reactions under irradiation potentially restrict the use of oxide in this capacity.[8] Since it had been reported that the uranium-aluminum intermetallics were stable under these conditions,[9] a limited amount of work was performed to determine

---

[7]J. I. Federer and C. F. Leitten, Jr., Fuels and Materials Development Program Quart. Progr. Rept. Dec. 31, 1964, ORNL-TM-1000, pp. 4–10.

[8]A. E. Richt, C. F. Leitten, Jr., and R. J. Beaver, "Radiation Performance and Induced Transformations in Aluminum-Base Fuels," p. 469 in Research Reactor Fuel Element Conference, September 17–19, 1962, Gatlinburg, Tennessee, TID-7642, Bk. 2 (1963).

[9]G. W. Gibson and D. R. de Boisblanc, "Uranium-Aluminum Alloy Powders for Use as Nuclear Reactor Fuels," paper presented at 1963 Fall Meeting of the Metallurgical Society of the AIME, Cleveland, Ohio, October 21–25, 1963.

the feasibility of intermetallic fuel and fuel plate preparation. These studies showed that high-performance, aluminum-base fuel plates containing either arc-cast UAl_2-UAl_3 mixtures or stoichiometric compounds produced by powder metallurgy processes could be fabricated into fuel plates by conventional techniques with no deleterious effects. This work will now be augmented by irradiation of the intermetallics in the form of ORR fuel elements. Because of the variable UAl_2-UAl_3 composition of material produced by casting, which severely restricts the production of large quantities of plates of equal fuel volume, powder metallurgy route UAl_3 was chosen for the subject application.

The UAl_3 was prepared in the following manner: High-purity uranium metal was hydrided to produce finely divided particles (3- to 4-μ average particle size). This material was then intimately mixed with the proper amount of high-purity aluminum powder (−325 mesh) by oblique dry blending. The blend was placed in a graphite die and the hydrogen removed from the mixture by the application of heat and vacuum. The mixture was then hot pressed under a partial pressure of high-purity argon at 1000°C for 2 hr. Figure 1.1 is a composite showing the microstructure of the UAl_3 hot pressing and longitudinal and transverse sections of a UAl_3 dispersion plate. The UAl_3 hot pressings were crushed to the proper particle size (−170 +325 mesh) by hand-crushing techniques. High-quality blister-free plates of appropriate dimensions were fabricated from these intermetallics using conventional picture-frame techniques.

Chemical, spectrographic, and x-ray analyses were performed on the starting, intermediate (UH_x), and final materials. These analyses showed no major impurities or impurity pickup during processing. Chemical and x-ray analyses of the starting materials and final sized product are shown in Table 1.2.

[redacted]

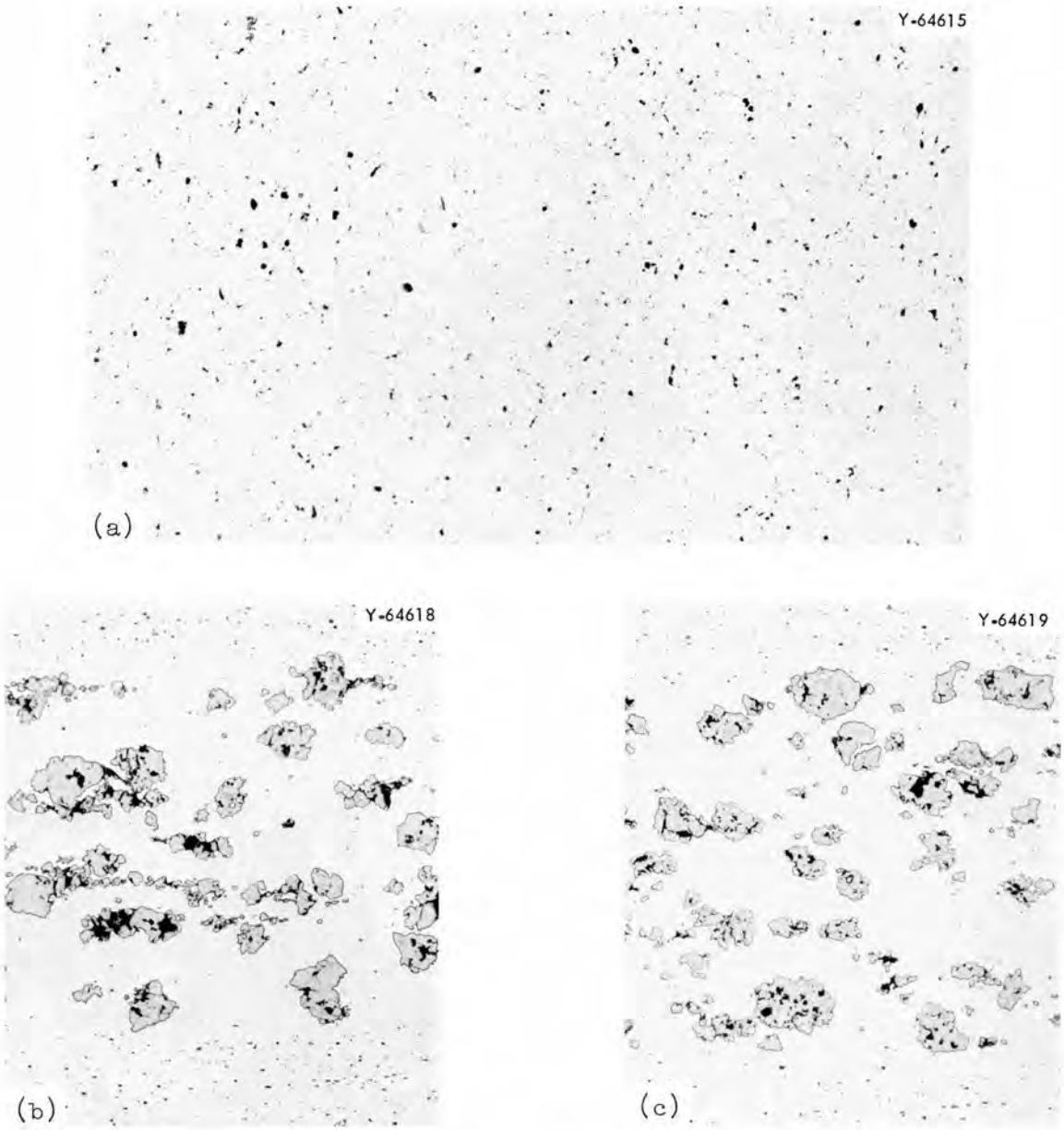

Fig. 1.1. Selected Photomicrographs of UAl_3 Production Stages and UAl_3 Dispersion Plate Cross Sections. 100× (a) Microstructure of UAl_3 pellets. Etchant: 5% concd HF. (b) Logitudinal section of rolled fuel plate. As polished. (c) Transverse section of rolled plate. As polished.

[redacted]

[redacted]

Table 1.2. Chemical and X-Ray Analyses of UAl_3 Starting Materials and Final Product

Parameter	Material		
	Al	U (metal ingot)	UAl_3 (powder)
O_2, %	0.24	0.018	0.1318
N_2, %	0.0041	0.0027	0.024
C, %	0.005	0.004	0.041
ρ(Toluene picnometer), g/cm^3			6.7369
BET surface area, m^2/g			0.20
g U/g UAl_3			0.72932
Moisture content, %	< 0.03		0.0361
Enrichment, % ^{235}U			93.19
X-ray UAl_3, %			95.97

[redacted]

2. MECHANICAL PROPERTIES

J. R. Weir, Jr.

One objective of this program is to determine the effect of irradiation on the mechanical properties of alloys of interest as fuel cladding and to find a metallurgical condition for the alloys that produces the least effect of subsequent irradiation on the mechanical properties. To accomplish this, our study concerns the interaction of radiation-induced defects and the substructure of the alloys, the effect of irradiation temperature, postirradiation test variables, and neutron dosimetry in the facilities used in the irradiations. The material selected for initial study is type 304 stainless steel. The stabilized grades are also being investigated because of the effects of niobium and molybdenum on the stability of substructures formed by cold working and annealing.

Irradiation Embrittlement of Low-Boron Type 304 Stainless Steel

W. R. Martin J. R. Weir, Jr. R. E. McDonald

There is a growing amount of literature[1–7] that describes the magnitude and characteristics of the irradiation-induced embrittlement of alloys at elevated temperatures. These data appear to be consistent

---

[1]N. E. Hinkle, "Effect of Neutron Bombardment on Stress-Rupture Properties of Some Structural Alloys," Am. Soc. Testing Mater. Spec. Tech. Publ. 341, 344 (1963).

[2]P. C. L. Pfiel and D. R. Harries, "Effect of Irradiation on Austenitic Steels and Other High Temperature Alloys," paper presented at the American Society for Testing and Materials Symposium on Flow and Fracture of Metals and Alloys in Nuclear Environment, Chicago, Ill., June 21–26, 1964 (to be published).

[3]W. R. Martin and J. R. Weir, "The Effect of Irradiation Temperature on the Postirradiation Stress-Strain Behavior of Stainless Steel," paper presented at the American Society for Testing and Materials Symposium on Flow and Fracture of Metals and Alloys in Nuclear Environment, Chicago, Ill., June 21–26, 1964 (to be published).

[4]A. N. Hughes, and J. R. Caley, J. Nucl. Mater. 10(1), 60 (1963).

[5]J. Fennell and A. C. Roberts, J. Nucl. Mater. 12, 167 (1964).

[6]W. R. Martin and J. R. Weir, "Effect of Elevated-Temperature Irradiation on Hastelloy N," to be published in Nuclear Applications.

[7]F. A. Comprelli, B. C. Beaudreau, H. J. Busboom, and C. N. Spalaris, Trans. Am. Nucl. Soc. 7(2), 455 (1964).

with the hypothesis that the grain boundary embrittlement is due to the helium generated by the ^{10}B (n, α) ^{7}Li thermal neutron capture reaction.[1,8,9]

This work is the result of a study of the effect of very small concentrations of boron on the irradiation embrittlement of type 304 stainless steel irradiated to a high exposure in a thermal neutron test reactor. These steels generally contain in excess of 1 ppm B and it was necessary to electron-beam remelt a commercial heat of steel to reduce the concentration of this element to very low values.

Five charges of approximately 650 g were prepared by cutting 1/4-in.-diam rod material into 2-in. lengths. The charges were melted using an 18-kw power level and melting times of 4, 8, 12, 16, and 20 min. The resulting "pancakes" were 4 in. in diameter and 7/16 in. thick. The chemistry of these pancakes is representative of the austenitic stainless steel class.

The boron concentration was determined using the spark source mass spectrograph of the Mattauch-Herzog geometry, which utilizes a radio frequency spark to produce ionization of the sample. The resulting ions are focused according to energy and direction and collected on an Ilford Q II photographic plate. Elements are identified by position on the plate and concentrations are estimated from the density of the line as compared with an internal standard. In all samples of this series, ^{53}Cr was used as an internal standard. Chromium-53 is a minor isotope and was free of any interference from other constituents of the sample. The samples were sparked so that a maximum exposure of 0.3 microcoulomb was obtained. For samples suspected, or known, to have high boron content, a 0.1-microcoulomb exposure was obtained. Detection limit varied from 5×10^{-9} to 8×10^{-8} atom fraction depending on exposure, plate, and sample. In

---

[8]R. S. Barnes, Some Mechanisms of Radiation Induced Mechanical Property Changes, United Kingdom Atomic Energy Authority Report AERE-R-4655 (July 1964).

[9]J. Moteff, F. C. Robertshaw, and F. D. Kingsbury, Effect of Neutron Irradiation on the Stress-Rupture Properties of High Temperature Precipitation Hardening Alloys, General Electric Report GE-TM 64-6-21 (May 1964).

no case was the boron concentration lower than the detection limit for that sample. Results are summarized in Table 2.1. These data are believed to be accurate to within ±50%.

Table 2.1. Boron Concentration by Weight

Alloy Number	Remelting Time in Furnace (min)	Natural Boron (ppm)	Detection Limit (ppm)
18141BC	0	3.90	0.016
EBM706	8	0.130	0.003
EBM707	12	0.015	0.003
EBM709	16	0.107	0.003
EBM710	20	0.023	0.001

After the various heats had been analyzed, the electron-beam melted alloys and the commercial heat (in the as-received condition) were machined into subsize tensile specimens which were then irradiated in the core of the Oak Ridge Research Reactor at a temperature of 700°C. The samples were then removed from the reactor and tension tested in a hot cell using an Instron machine. The postirradiation ductilities, as given by the true uniform strain and total elongation, are listed in Table 2.2 for deformation at 704 and 842°C.

Only small variations are found in the ductilities of all the electron-beam melted heats, although an order of magnitude exists between the concentrations of boron. The largest difference in ductility exists between the commercial alloy and the electron-beam remelted alloys. The concentrations of helium were calculated for the ^{10}B (n, α) reaction for each of the alloys and are given in Table 2.3. If one considers only the (n, α) reactions due to thermal neutrons, these data suggest that helium is not responsible for the embrittlement or that the embrittlement is quite independent of helium concentrations in the range of 0.13 to 1.1×10^{-7} atom fraction. However, if one computes the concentration of helium due to fast neutron (n, α) reactions for all the elements present in stainless steel, then these data appear more

[redacted]

Table 2.2. Embrittlement of Stainless Steel Irradiated at 700°C

Tensile Test Temperature (°C)	Natural Boron Concentration (ppm)	Ductility[a] (%)			
		True Uniform Strain[b]		Total Elongation	
		Irradiated	Unirradiated	Irradiated	Unirradiated
704	0.015	13.7		19.1	
	0.023	12.7	30.9	23.3	56.2
	0.107	13.1		21.6	
	0.130	12.7	19.6	19.6	60.4
	3.9	11.2	18	13.1	40.2
842	0.015	3.1		6.1	
	0.023	2.9		6.1	
	0.107	2.9	13.8	5.6	46.6
	0.130	3.3	18.2	6.1	57.2
	3.9	1.5	16.0	3.0	43.0

[a]Irradiated at B-8 position of the Oak Ridge Research Reactor to a neutron dose of 4.5×10^{20} neutrons/cm^2 (thermal) and 3.5×10^{20} neutrons/cm^2 ($E > 1$ Mev).

[b]Specimens strained at a rate of 0.2%/min.

Table 2.3. Approximate Helium Concentration from all (n, α) Reactions

Alloy Number	Natural Boron Concentration (ppm)	Helium Concentration (Atom Fraction)		
		Due to ^{10}B and Thermal Neutrons	Due to Fast Neutron (n, α) Reactions	Total
		$\times 10^{-6}$	$\times 10^{-6}$	$\times 10^{-6}$
EBM707	0.015	0.013	0.3	0.313
EBM710	0.023	0.020	0.3	0.320
EBM709	0.107	0.091	0.3	0.391
EBM706	0.130	0.110	0.3	0.410
18141BC	3.9	3.3	0.3	3.6

[redacted]

compatible with an irradiation embrittlement mechanism based on helium. The concentration of helium due to the (n, α) reactions with fast neutrons is also given in Table 2.3; these data were taken from the work of Bush, Moteff, and Weir.[10] Considering the helium from all sources, the lack of variation in ductility of the electron-beam melted heats is more easily explained since the difference in total helium concentration is less than a factor of 2. This suggests that the irradiation of these electron-beam melted alloys in a more thermal neutron environment or to a lower fast neutron dose would result in a greater variation in the ductilities. This is indeed the case as shown in Table 2.4.

It is concluded that removing the ^{10}B from the alloy is not the ultimate solution for improving the ductility of irradiated alloys because even in thermal neutron reactors, (n, α) reactions with fast neutrons are important, particularly for materials containing low boron concentrations.

Irradiation Embrittlement of Stainless Steel at Very High Temperatures

W. R. Martin J. R. Weir, Jr.

We have previously shown[11] that the postirradiation ductility of type 304 stainless steel at elevated temperatures is practically independent of irradiation temperature up to 700°C. Our studies of irradiation temperature have now been extended into the temperature range of 700 to 900°C.

Two heats of stainless steel were irradiated, one containing 0.02 wt % C and the other containing 0.06 wt % C. Subsize tensile specimens were machined from 1/4-in.-rod stock and irradiated in the Oak Ridge Research Reactor at temperatures of 700, 800, and 900°C. The

---

[10]S. H. Bush, J. Moteff, and J. R. Weir, "Radiation Damage in Fast Reactor Components," presented at the American Nuclear Society Topical Meeting on Fast Reactor Technology, Detroit, Michigan, April 26–28, 1965 (to be published).

[11]W. R. Martin and J. R. Weir, "The Effect of Irradiation Temperature on the Postirradiation Stress-Strain Behavior of Stainless Steel," paper presented at the American Society for Testing and Materials Symposium on Flow and Fracture of Metals and Alloys in Nuclear Environment, Chicago, Ill., June 21–26, 1964 (to be published).

Table 2.4. Effect of Boron Content on Type 304 Stainless Steel at High and Low Doses

Irradiation Dose (neutrons/cm^2)	Boron Content (ppm)	Elongation (%)		Helium Concentration (ppm)		Total
		704°C	842°C	^{10}B (n, α)	Fast (n, α)	
Approximately 5×10^{20}	0.11	22	6	0.091	0.3	0.391
	3.9	13	3	3.3	0.3	3.6
Approximately 5×10^{16}	0.11	39	41	0.00004	0.00006	0.0001
	3.9	40	29	0.00150	0.00006	0.0015

ductilities, as given by the true uniform strain and total elongation on testing at 650, 704, 775, and 842°C, are listed in Table 2.5 for the irradiated and the unirradiated control specimens.

The preirradiation ductilities of the low- and high-carbon steels were not significantly different. However, except for irradiation at 900°C, the postirradiation ductility of the high-carbon heat was significantly better than the low-carbon heat. In general, the ductility of the irradiated alloy decreases when either the testing temperature or the irradiation temperature is increased. Deformation temperature appears to have a greater influence than irradiation temperature. The influence of irradiation temperature might be associated with grain growth or carbon redistribution, and hence, the largest effect is noted at 900°C, the temperature at which all the carbon is in solution in the high-carbon heat.

The higher ductilities observed for the high-carbon alloy may be due to several factors. The concentration of the helium generated from (n, α) reactions is approximately 20% lower in the high-carbon heat due to smaller concentration of ^{10}B (0.6 to 0.8 ppm). However, we believe that the improved ductility is related to the distribution and agglomeration of grain-boundary carbides. Weaver[12,13] has shown that heat treatment of a nickel-base alloy, to produce a coherent precipitate in the grain boundaries, improved the ductility. If the strength of the carbide-matrix interface is large compared to the cohesive strength of the boundary, grain-boundary precipitates that reduce the length of the sliding interface can increase the stress necessary to cause triple-point cracks. Weaver observed that the precipitate in the nickel-base alloy restricted the propagation of these cracks to intercarbide spaces.

One can apply this reasoning to the variation of irradiation embrittlement observed for the 0.02 wt % C and the 0.06 wt % C stainless steels. Hence, if the high-carbon steel is given a preirradiation heat treatment

---

[12] C. W. Weaver, J. Inst. Metals 88, 296 (1959–60).

[13] C. W. Weaver, Acta Met. 8, 343 (1960).

Table 2.5. Elevated Temperature Ductility of Unirradiated and Irradiated AISI Types 304L and 304 Stainless Steels

Deformation Temperature (°C)	Irradiation Temperature[a] (°C)	Carbon Content (wt %)	True Uniform Strain[b] (%)		Total Elongation (%)	
			Unirradiated	Irradiated	Unirradiated	Irradiated
650	700	0.02	22.5	15.1	42.2	16.9
	700	0.06	20.9	21.8	36.8	28.5
	800	0.02	23.6	13.1	39.8	17.6
	800	0.06	22.2	20.5	41.7	29.9
	900	0.02		10.5		11.3
	900	0.06	23.7	11.4	37.4	12.4
704	700	0.02	17.7	11.2	38.9	13.1
	700	0.06	17.8	17.1	41.5	23.0
	800	0.02	18.0	11.2	36.2	13.3
	800	0.06	14.0	14.1	36.6	20.3
	900	0.02	17.8	6.1	31.4	6.4
	900	0.06	17.4	14.6	28.0	
775	700	0.02	10.2	7.1	33.0	9.1
	700	0.06	10.4	9.6	40.7	15.7
	800	0.02	10.0	5.0	30.0	7.2
	800	0.06	9.3	7.6	40.0	12.6
	900	0.02		2.5		2.9
	900	0.06	14.1	3.4	31.7	4.0
842	700	0.02	9.8	4.8	38.4	6.7
	700	0.06	7.0	6.3	31.9	10.6
	800	0.02	10.4	2.8	36.8	4.0
	800	0.06	10.4	5.8	39.0	8.8
	900	0.02	10.2	1.8	24.5	2.2
	900	0.06	10.8	2.4	25.6	3.0

[a]Alloys irradiated to a neutron dose of 3.5×10^{20} neutrons/cm^2 ($E > 1$ Mev) and 4.5×10^{20} neutrons/cm^2 (thermal).

[b]Specimens strained at a rate of 0.2%/min.

to agglomerate the carbides, the ductility is improved. Examples are given in Table 2.6.

Table 2.6. Effect of Grain-Boundary Carbides on Elevated Temperature Embrittlement of Irradiated Stainless Steel[a]

Deformation Temperature (°C)	True Uniform Strain[b] (%)	Total Elongation (%)	Preirradiation Heat Treatment[c]
704	15.6	20.5	Alpha
704	18.1	30.5	Beta
842	5.1	7.6	Alpha
842	9.4	13.9	Beta

[a]Heat 33107 (0.06 wt % C) irradiated at 50°C for a neutron dose of 7×10^{20} neutrons/cm^2 ($E > 1$ Mev) and 9×10^{20} neutrons/cm^2 (thermal).

[b]Specimens strained at a rate of 0.2%/min.

[c]Alpha denotes solid-solution anneal at 1036°C for 1 hr, and beta denotes solid-solution anneal at 1036°C for 1 hr followed by aging treatment of 100 hr at 800°C.

It has been found that irradiation temperatures above 800°C significantly affect the ductility of types 304L and 304 stainless steels. It is believed that the variations in ductility of the irradiated low- and high-carbon steels are due to grain-boundary carbides that affect the process of intergranular fracture. The agglomeration of carbides at the grain boundary tends to reduce the embrittlement caused by the (n, α) reactions.

The use of this heat-treatment technique to improve the ductility of cladding materials for high-temperature application will depend upon the thermal stability of the agglomerated precipitate.

Ductility of Irradiated 18-8 Type Stainless Steels Containing Titanium

W. R. Martin J. R. Weir, Jr.

It is presently believed that the cause of the radiation-induced grain-boundary embrittlement in iron- and nickel-base alloys is the

generation of helium due to (n, α) reactions. Helium bubbles at the grain boundary would be expected to be deleterious. However, helium generated within the grains would not be as harmful. The only way these helium atoms could be swept into the boundary would be by a dislocation mechanism as illustrated by Barnes for copper. Therefore, to improve the ductility of irradiated materials, one must devise ways to reduce the helium concentration at the grain boundaries. Some metallurgical factors, such as grain size,[14] have already been investigated and reported previously.

For many reactor applications, the preponderance of helium generated is due to the transmutation of ^{10}B. Boron normally segregates to the grain boundaries in the solid state and therefore a large quantity of helium is generated at these boundaries. If one could form a stable boron compound, insoluble either in the melt or at a very high temperature after solidification, it would be possible to get a homogeneous distribution of this compound. Therefore, helium generated would tend to stay at the precipitate-matrix interface and hence the quantity at the grain boundaries would be greatly reduced. These precipitates having an incoherent interface, would also serve as a depository for helium generated from other elements and fast neutrons. Thus in principle, this system should result in material with a lower susceptibility to elevated-temperature embrittlement in thermal and fast neutron environments.

We have chosen to first investigate the iron-base systems, in particular the 18-8 stainless steel. Among the most stable borides are those of titanium. We have now accumulated data from two different irradiations and typical data are given in Table 2.7 for a steel containing 0.06 wt % C. It is clear that small additions of titanium greatly improve the ductility of type 304 stainless steels. Titanium additions at the level required to meet the chemical specifications for type 321 stainless steel are above the range for which one gets the maximum ductility.

---

[14]W. R. Martin and J. R. Weir, Influence of Grain Size on the Irradiation Embrittlement of Stainless Steel at Elevated Temperatures, ORNL-TM-1043 (March 1965).

Table 2.7. Influence of Titanium on the Elevated-Temperature Irradiation Embrittlement of 18-8 Stainless Steels

Titanium (wt %)	Total Elongation (%)[a,b]		
	650°C	700°C	842°C
0.0	31.0	31.5	20.0
0.2	40.0	38.0	45.1
0.3	34.7	28.5	35.2
0.4	31.5	26.5	25.0
0.5	28.8	21.5	19.0
0.6	24.1	19.5	17.9
0.8	22.9	20.5	19.1
1.0	30.6	23.5	23.5
1.2	29.8	23.0	28.5

[a]Measured in 1-in.-gage length for tests at a strain rate of 0.2%/min.

[b]Specimens irradiated to a dose level of 1×10^{20} neutrons/cm^2 (thermal) and 1.5×10^{19} neutrons/cm^2 ($E > 1$ Mev).

Titanium additions in the range up to 0.2 wt % greatly reduce the magnitude of irradiation embrittlement in type 304 stainless steel. Although the alloys containing titanium have a grain size smaller than the unstabilized grade, we believe the effect of titanium to be as hypothesized earlier. We plan to investigate the properties of this alloy in more detail.

3. NONDESTRUCTIVE TEST DEVELOPMENT

R. W. McClung

Our program is intended to develop new and improved methods of evaluating reactor materials and components. To achieve this we have studied various physical phenomena, developed instrumentation and other equipment, devised application techniques, and designed and fabricated reference standards. Among the methods being actively pursued are electromagnetics (with major emphasis on eddy currents), ultrasonics, and penetrating radiation. In addition to our programs oriented toward the development of methods, we are studying these and other methods for evaluation of problem materials and developing techniques for remote inspection.

Electromagnetic Test Methods

C. V. Dodd

We have continued research and development on electromagnetic phenomena on both an analytical and an empirical basis. As part of the program, we are studying the methematical determination of impedance of an eddy-current coil and other electromagnetic field parameters as a function of coil dimensions, frequency, specimen conductivity and permeability, and coil-to-specimen spacing (lift-off). The relaxation techniques allow the solution of the electromagnetic boundary value problem on a digital computer. The differential equation for the field is approximated by finite difference terms. By making a number of correcting calculations, the value of the field can be made to converge to agreement with the differential equation at every point.

We have applied this technique to the problem of a long coil above a conducting plane. Figure 3.1 shows the variations in the phase and amplitude of the vector potential throughout the electromagnetic field. This is also representative of variations of the phase and amplitude of the current inside the metal since the current is proportional to the vector potential. After we have determined the vector potential, we can calculate any physically observable phenomenon such as the coil

[redacted]

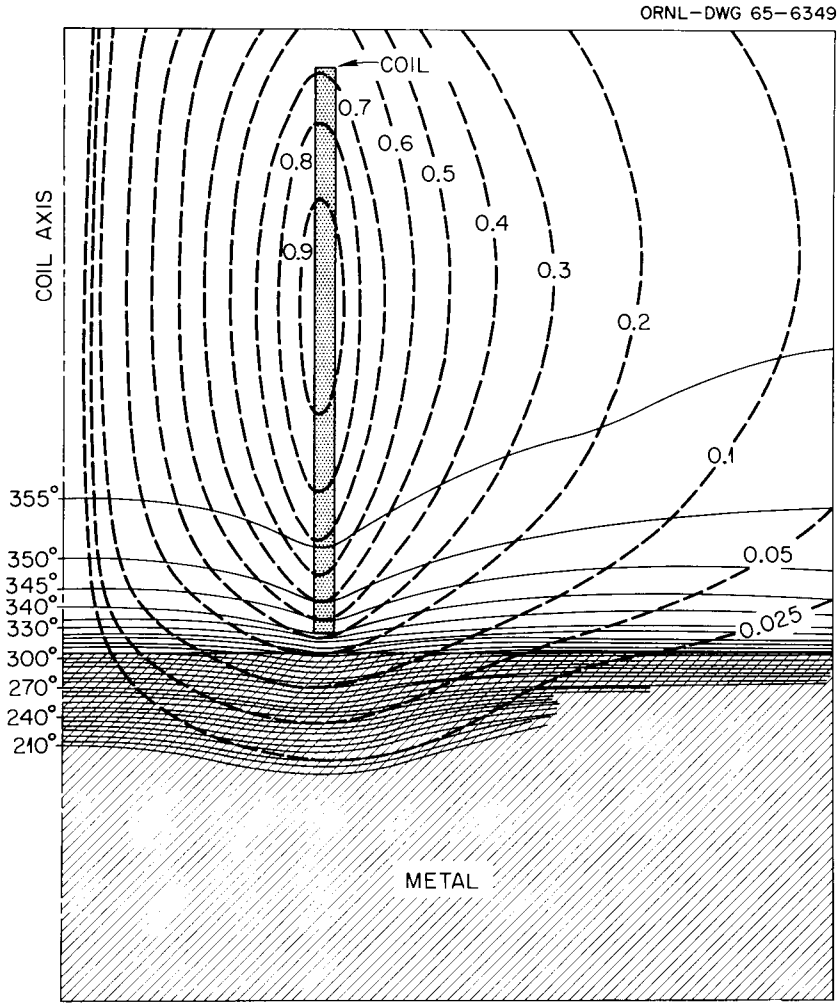

Fig. 3.1. Phase and Amplitude of the Vector Potential of a Coil Above a Metal Plane.

impedance, the current in the metal, the rate of ohmic heating at any point, or the eddy-current forces on the metal. Figure 3.2 shows contours of equal heating density for the coil mentioned above.

We have derived new relaxation equations to calculate the vector potential due to current pulses. With these new equations we can perform calculations for magnetic materials with nonlinear permeability. In addition we have derived the appropriate equations to calculate both the eddy-current forces and the magnetic forces on metals. These new equations are being programmed for computer solution.

[redacted]

[redacted]

ORNL-DWG 65-6348

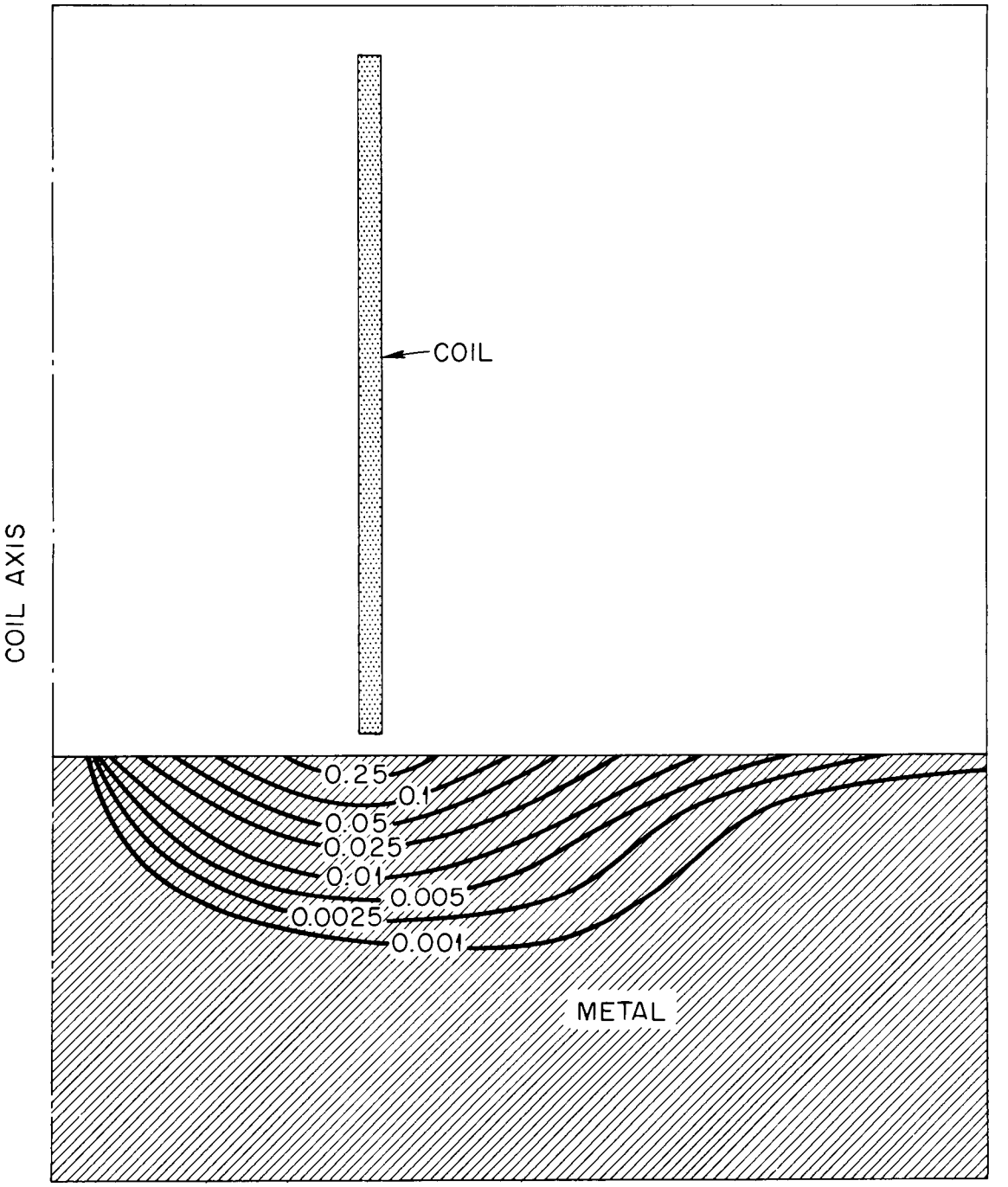

Fig. 3.2. Contours of Eddy-Current Heating Density.

[redacted]

Ultrasonic Test Methods

K. V. Cook

Nonbond Studies

We have continued our studies on the behavior of ultrasound in thin sections with the principal effort being the detection of nonbonds in cladding structures. As reported previously,[1] the basic through-transmission technique developed to detect nonbonds in thin fuel plates by monitoring changes in transmitted intensity has been applied successfully to the evaluation of fuel tubes. This method utilizes a two-transducer through-transmission technique and can be conveniently applied in a "cold" (radiation level) laboratory. However, it is desirable to evaluate such fuel elements in a "hot" laboratory using remote handling methods. Preliminary mockup studies have shown that a modified through-transmission ultrasonic inspection is feasible and could simplify the mechanical "jigging" requirements. This method employs one transducer which serves as both transmitter and receiver. The ultrasonic energy is transmitted through the tube wall, across the inside of the tube (which is filled with water), reflected from the inner surface of the opposite tube wall and thence, back along the same path to the receiver. Thus, any nonbond will attenuate the sound as it is transmitted through the wall in both directions.

We made studies to determine optimum sizes for calibration, transducer-to-specimen distance, etc. The data are being used to fabricate a Teflon guide block which will maintain proper alignment between the transducer and the specimen during evaluation.

---

[1]K. V. Cook, Fuels and Materials Development Program Quart. Progr. Rept. March 31, 1965, ORNL-TM-1100, p 20.

Tubing Inspection

Reference Standards. — We are continuing to work on the problems encountered in tubing inspection. A major problem is the establishment of realistic ultrasonic notch standards for calibration. Since electrical-discharge machining appears to be a reliable method for making both inner- and outer-surface notches, we are continuing our fabrication studies.[2] Calibration curves for machining of notches in FS-85, D-43, B-66, T-111, and titanium have been generated. Further work is planned on different materials so that similar tool feed-to-notch depth curves can be established for each. Also, we hope to decrease the width of our notches until they more nearly resemble cracks. We are developing techniques for machining notches on the inner surface of tubing with very small diameters. Thus far the smallest inner diameter on which electrical-discharge machine notches have been placed is approximately 0.085 in.

Tapered Tubing. — In a continuation of work begun in support of a NASA subcontract, we have successfully developed and applied ultrasonic techniques for the detection of defects in tapered nuclear heat exchange tubing. A paper[3] on this subject has been prepared and the abstract is included here as a portion of our contribution to this report:

> In order to obtain improved performance from heat exchangers, many nuclear engineers are considering the use of tubing that has a constantly varying diameter along its length, thus producing a tapered configuration. Some of the tubing exhibits a reverse taper (i.e., its diameter varies from large at one end to small near the center and back again to large on the other end). Until recently, the available inspections were inadequate for the detection of discontinuities in the tapered tubing. However, recent

---

[2]K. V. Cook, Fuels and Materials Development Program Quart. Progr. Rept. Dec. 31, 1964, ORNL-TM-1000, pp 39–41.

[3]R. W. McClung and K. V. Cook, "Development of Ultrasonic Inspection Techniques for Tapered Tubing," submitted to Materials Evaluation.

development of ultrasonic techniques and equipment at the Oak Ridge National Laboratory has provided a useful solution for this inspection problem.

Development of a mechanical scanning system allowed proper ultrasonic beam orientation to be maintained despite the diameter varying as a scan was made. Associated circuitry provided an audible alarm and a "B" scan presentation to denote the presence of discontinuities. This system has been successfully applied to the inspection of both 0.009-in.- and 0.050-in.-wall tapered tubing. Sensitivity to discontinuities 0.0005 in. in depth was demonstrated for the thin wall tubing.

Penetrating Radiation Methods

Gamma Scintillation Gaging — B. E. Foster, S. D. Snyder

We are continuing the study of x- and gamma-ray attenuation to the evaluation of fuel elements. Variation in transmitted intensity can be monitored readily by scintillation gaging and can be related through proper calibration to the fuel loading homogeneity within the area of the fuel beam. Our recent work has used the newly fabricated fuel rod scanner [4] To provide a basic calibration, we have scanned two vibratorily compacted Th—3 wt % UO_2 fuel rods (1/2 in. in diameter) and six ThO_2 pellets contained in a 3/4-in -diam tube using ^{60}Co and ^{137}Cs as the radiation sources. With each of the sources these specimens were scanned at longitudinal speeds of 2, 4, 8, 12, 16, 20, and 24 in./min — one series of scans with a 1/8- × 1/8-in. collimator and another series with a 1/8- × 1/2-in. collimator. Data processing is in progress. Prior to the aforementioned scanning we learned that shielding between the two source beams was inadequate, so that a severe "cross-talk" was present. Additional shielding was provided by mounting lead-shot-filled rectangular aluminum cans to each collimator in a fashion that will still permit easy interchange of collimators without the removal of the shields.

X-Ray Projection Microscopy — W. H. Bridges

The various electron-optical components for the x-ray projection microscope have been assembled and tested in several different

[4] B. E. Foster and S. D. Snyder, Fuels and Materials Development Program Quart. Progr. Rept. Dec. 31, 1964, ORNL-TM-1000, pp 41—44.

configurations in order to determine the optimum operating conditions of highest current density in the smallest spot. So far, with an accelerating voltage of 10 kv, electron beams of only 3 μa have been obtained with a spot size visually estimated to be approximately 20 μ. Increasing the accelerating voltage increased the beam current and, unfortunately, also the spot diameter. The target for x-ray generation was entirely too thick to give enough x rays to determine the resolution of the system at the low voltage. A target structure is now being built which will allow the changing of targets during operation so that an optimum thickness and/or material can be introduced. With this structure it should be possible to maximize the x-ray output with a minimum spot size.

Inspection Development of Problem Materials

K. V. Cook

We have continued to work on nondestructive tests for unusual materials that are difficult to inspect and/or new materials that have no evaluation history. This has included refractory metals including tungsten-, tantalum-, titanium-, and niobium-base alloys. A portion of this work is reported under "Ultrasonic Test Methods" in this chapter.

[redacted]

4. ZIRCONIUM METALLURGY

M. L. Picklesimer

We are conducting research along several lines on zirconium-base alloys of potential use as structural materials for water-cooled and/or -moderated reactor systems. The principal projects are: (1) studies of the physical metallurgy, including transformation kinetics and morphologies, mechanical properties, phase diagrams, and heat-treatment response; (2) the development, evaluation, and utilization of preferred orientation and strain anisotropy in α-zirconium alloys during fabrication, and the utilization of yield stress anisotropy in increasing maximum permissible design stresses in structures; (3) the determination of the effects of composition, temperature, and environment on the oxidation-corrosion rates in the thin-film stages of oxide growth; (4) a study of the effects of alloy composition and oxidation environment on the structural properties of thin oxide films *in situ*; and (5) investigation of stress orientation of hydrides in Zircaloy-2.

Effect of Preferred Orientation and Stress on the Directional Precipitation of Hydrides in Zircaloy-2

P. L. Rittenhouse

Since the last report on this project,[1] all the tests have been completed and the hydride pole figures have been determined. An ORNL report is being prepared to give the data in detail. In summary, specimens of Schedule J Zircaloy-2 plate[2] were hydrided to 120, 170, and 280 ppm H_2 (previously reported[1] as 50, 150, and 250 ppm), homogenized, and slow cooled to room temperature. They were then reheated to 400°C in air, loaded elastically to stress levels of 8,000, 14,000, or

---

[1]P. L. Rittenhouse, Fuels and Materials Development Program Quart. Progr. Rept. Sept. 30, 1964, ORNL-TM-960, pp. 38–41.

[2]P. L. Rittenhouse and M. L. Picklesimer, Metallurgy of Zircaloy-2 Part I. The Effects of Fabrication Variables on the Anisotropy of Mechanical Properties, ORNL-2944, p. 15 (Oct. 13, 1960).

[redacted]

[redacted]

20,000 psi, and furnace cooled to room temperature under stress. Gage section measurements, before and after stressing, showed that no plastic strain was detectable. This material had a strong concentration of basal poles oriented in the transverse direction of the rolled plate, permitting test specimens to have tensile stresses perpendicular to the basal plane as well as parallel to it.

Quantitative metallographic measurements were made of the hydride particle density and volume fraction on each surface of the specimen after stressing. Each specimen was anodized to permit positive identification of all hydrides. Particle number counts were made at 650× and volume fraction measurements at 1200×. There was no effect of stress level on either the particle size or the number of particles per square centimeter of surface area at any given hydrogen content. The data are shown in Figs. 4.1 and 4.2. The average area per particle calculated from the areal fraction and the number of particles per square centimeter were 7.5, 7.8, and 8.5 × 10^{-8} cm^2 for 120, 170, and 280 ppm H_2, respectively.

ORNL-DWG 65-6540

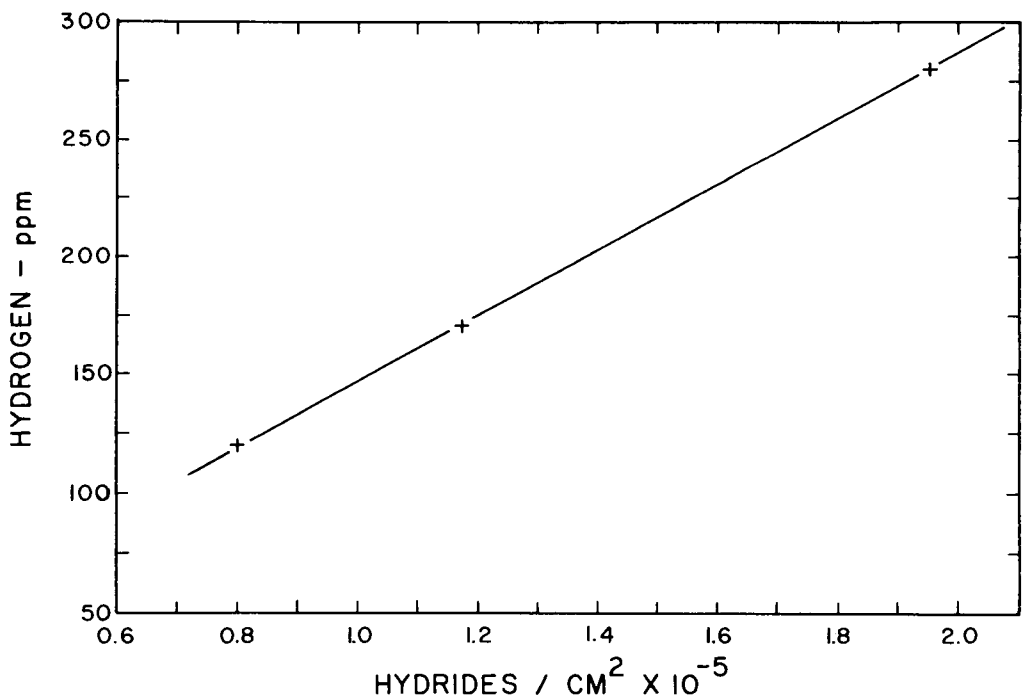

Fig. 4.1. Number of Hydride Particles vs Hydrogen Content in Zircaloy-2.

[redacted]

[redacted]

ORNL-DWG 65-6541

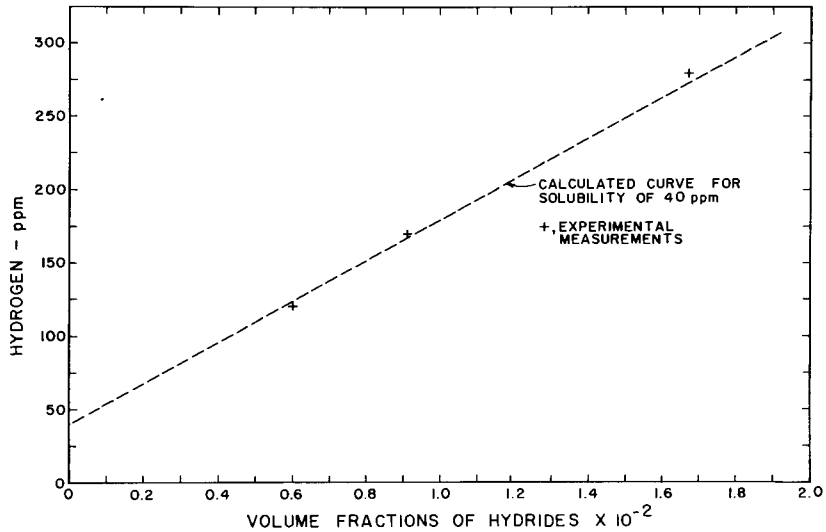

Fig. 4.2. Volume Fraction of Hydride vs Hydrogen Content in Zircaloy-2.

The hydride pole figures were determined by a quantitative metallographic technique, described in the following section of this chapter. A typical pole figure set is presented in Fig. 4.3 and shows the effects of both stress direction and hydrogen content on the preferred orientation of the hydrides.

The conclusions were:

1. The number of hydrides at any angle in the unstressed control specimens was a function only of hydrogen level, the percent of the total at each angle being identical for all three levels of hydrogen.

2. The conclusion, reported previously, that appreciable redistribution of hydrides precipitated under elastic stress occurs only when that stress is parallel to a concentration of basal poles greater than random seems to be confirmed.

3. The redistribution of hydrides increased as the stress increased.

4. A stress of 20,000 psi parallel to the basal poles causes the reorientation of hydride plates that were parallel to the stress to a position approaching perpendicularity to that stress.

5. In stressed specimens there may be preferred sites for precipitation that are filled at low hydrogen levels, and that higher hydrogen levels force less favorable sites to be occupied.

[redacted]

[redacted]

ORNL-DWG 65-6031

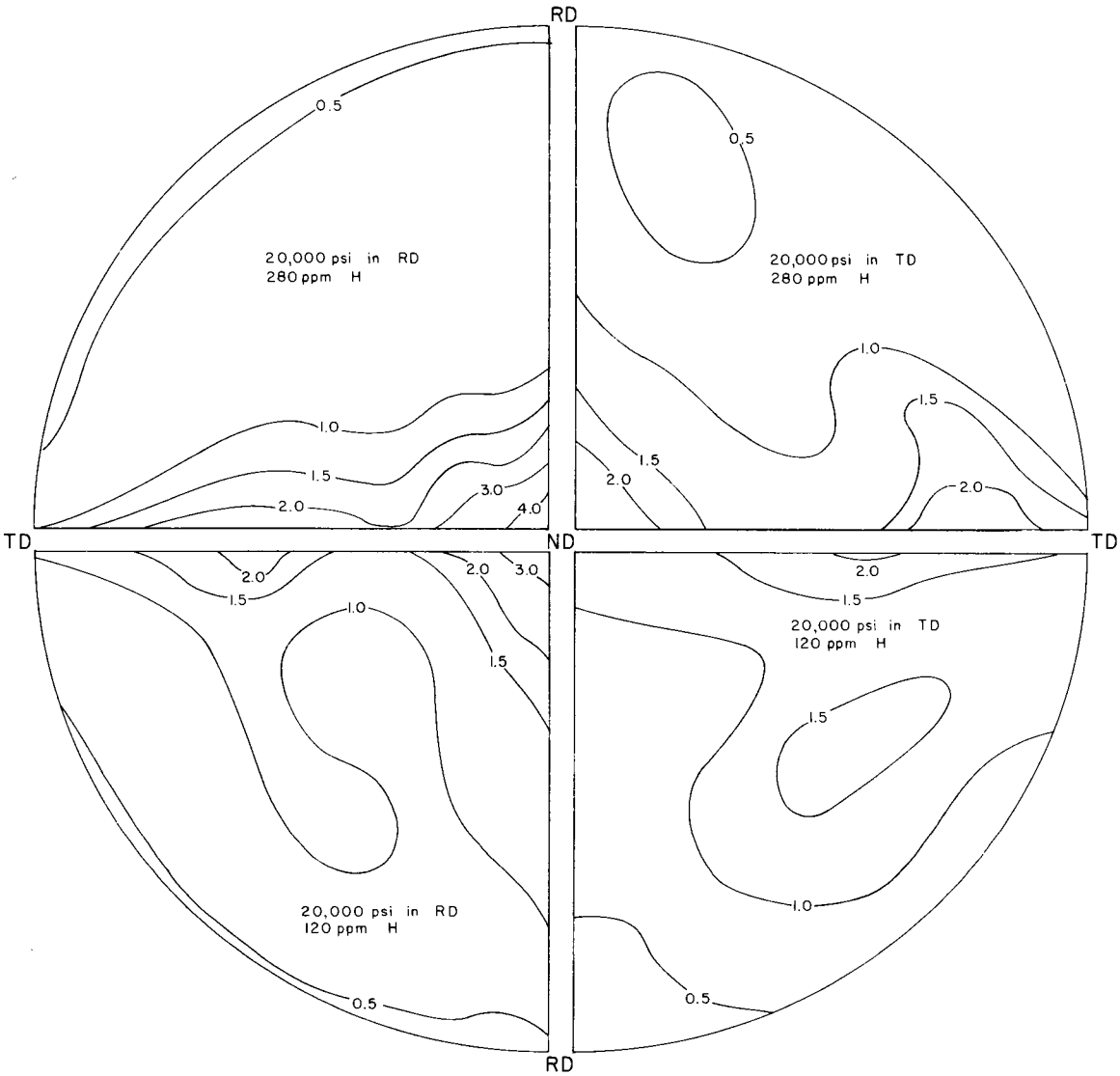

Fig. 4.3. Hydride Pole Distributions in Zircaloy-2. Tensile stress applied at 400°C; specimens furnace cooled under load.

[redacted]

[redacted]

6. The higher the hydrogen content, the greater is the number of hydrides stress oriented, but the fraction so oriented is less.

Hydride and Basal Pole Figures in Zircaloy-2 by Quantitative Metallography[3]

M. L. Picklesimer P. L. Rittenhouse

A technique has been developed for rapidly determining, by quantitative metallography, the pole figure of hydride plates in Zircaloy-2 and the basal pole figure of close-packed hexagonal metals. Approximately 200 trace angles are measured on each of three orthogonal surfaces, and smoothed histograms of the data are plotted. A trial-and-error solution of the pole figure is made from these, using the approximation procedure developed for determining pole figures from x-ray diffraction data. An eyepiece goniometer equipped with electrical readout of angle is used to measure the angle between specific reference directions and the traces of hydride plates on the specimen surfaces. A polarized-light metallurgical microscope equipped with a sensitive tint plate and electrical readout of stage angle is used for determining the basal plane trace in close-packed hexagonal metals. The trace angle data are collected on an x-y recorder with a remote pen action at a rate of 500 to 800 points per hour. Normally, the pole figure can be determined with sufficient accuracy in less than 2 hr on metallographically prepared specimens.

Tube Testing Apparatus

P. L. Rittenhouse M. L. Picklesimer

The tube testing apparatus designed for studying the anisotropy of strain in biaxial stress in Zircaloy-2 tubing has been completed. A schematic diagram of the apparatus was presented in a prior report.[4]

---

[3]Abstract of paper presented at the 19th Atomic Energy Commission Metallographic Group Meeting, Oak Ridge National Laboratory, April 20–22, 1965 (proceedings to be published as ORNL-TM-1161).

[4]P. L. Rittenhouse and M. L. Picklesimer, Fuels and Materials Development Program Quart. Progr. Rept. Dec. 31, 1964, ORNL-TM-1000, pp. 66–67.

[redacted]

Several preliminary tests have been made in the debugging program. At this time, the programming, control, and recording systems for simultaneous tension and torsion are satisfactorily operational. The internal pressure system and the internal volume measurement system are now being tested. Full-scale testing of Zircaloy-2 tubing is expected within the next month, provided no major changes are required in the internal pressure and volume systems.

Optical Properties of Zirconium Alloys

L. T. Larson[5] M. L. Picklesimer

The reasons for and the experimental techniques used in the study of the optical properties of zirconium and its alloys were discussed in a prior report of this series.[6] The measurements discussed there were made on small flat specimens which were difficult to prepare and align under the microscope. A single-crystal sphere of zirconium, approximately 9/16 in. in diameter was prepared. It is sufficiently smooth, round, and aligned in the five-axis stage constructed for this study[6] for the surface to remain in focus at 220× over more than three-fourths of its surface within one-half turn of the fine focus screw of the microscope.

Measurements were made of the angle of rotation, A_r, of the polarized light by the specimen as a function of crystallographic plane and wavelength of incident light. The data are presented in two ways in Figs. 4.4 and 4.5. The precision of measurement is such that any individual point on these figures is in error by no more than ±0.05 deg of A_r for wavelengths greater than approximately 490 mμ, ±2 mμ wavelength, or ±1/2 deg of crystallographic angle (there is a possibility that all of the numbers for crystallographic data are in error by as much as 3 deg in the same direction, due to an inaccurate determination of the

[5]Consultant, Department of Geology, University of Tennessee.

[6]L. T. Larson and M. L. Picklesimer, Fuels and Materials Development Program Quart. Progr. Rept. Sept. 30, 1964, ORNL-TM-960, pp. 41–43.

[redacted]

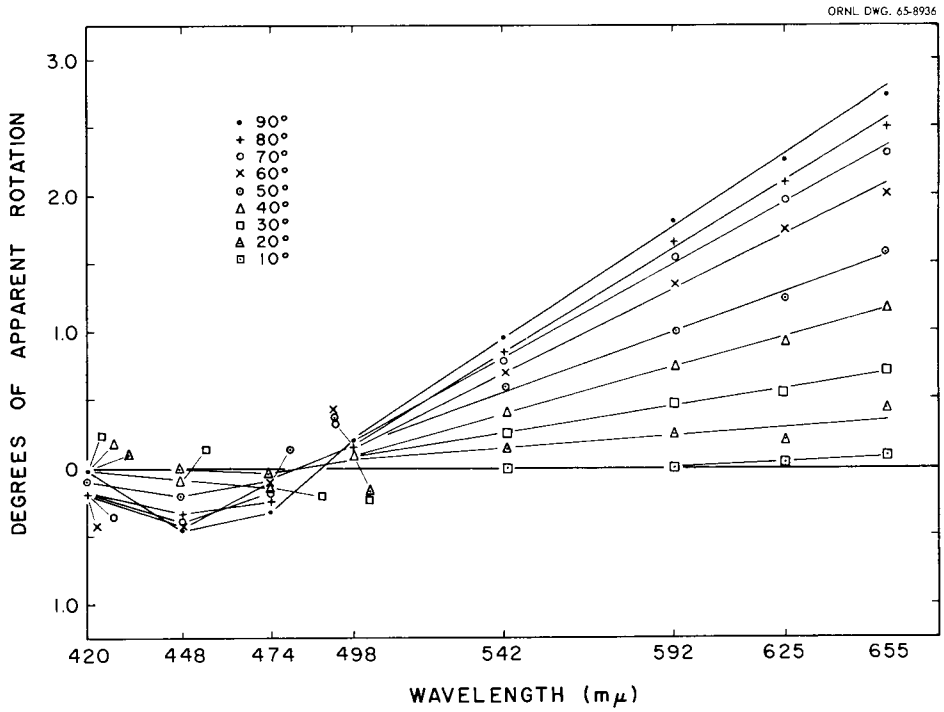

Fig. 4.4. Angle of Rotation of Polarized Light in Zirconium as a Function of Wavelength and Angle Between the Basal Pole and the Surface Normal. Single-crystal sphere, monochromatic light, and normal incidence.

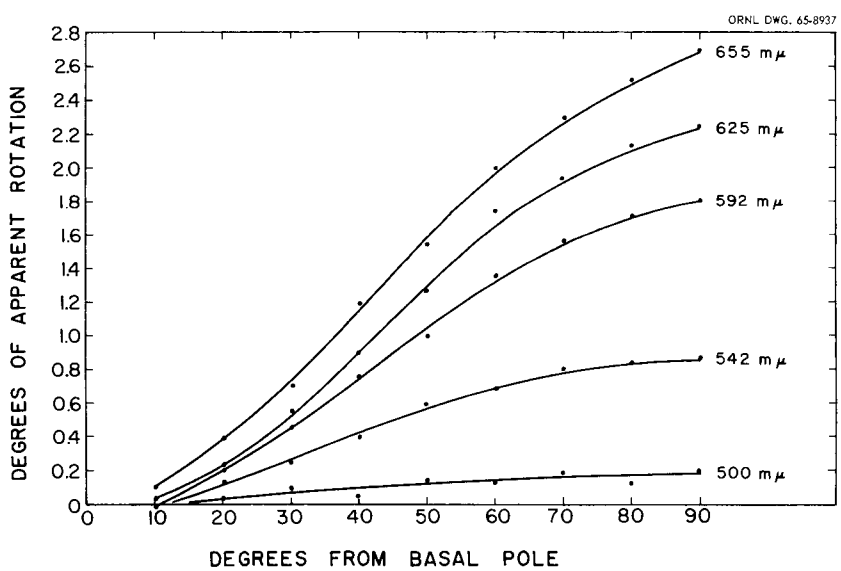

Fig. 4.5. Angle of Rotation of Polarized Light in Zirconium as a Function of Angle Between the Basal Pole and the Surface Normal. Single-crystal sphere, monochromatic light, and normal incidence.

[redacted]

basal pole position; the relative error still remains no more than ±1/2 deg). At wavelengths less than 490 mμ, the possible error in A_r is closer to ±0.1 deg, since the sensitivity of the human eye at these wavelengths is less than that at the longer wavelengths. A disk fluorescing at about 590 mμ when illuminated with shorter wavelength light is being prepared to increase our accuracy in measurement in the shorter wavelength region of the visible spectrum.

With reference to the data presented in Fig. 4.4, the value of A_r seems to be a linear function of wavelength between 542 and 655 mμ for all crystallographic planes. The exact relationships for wavelengths less than 542 mμ cannot be determined until more precise measurements can be made.

The relationships between the angle of rotation and the angle between the basal pole and the pole of the plane of examination (crystallographic plane) is shown in Fig. 4.5 for several wavelengths of monochromatic light. Use of the data at either 655 or 625 mμ wavelength will permit the determination from a single-surface examination of the tilt of the basal pole from the normal to the surface of the specimen to within about ±3 deg (the error in determination of the angle of rotation is < ±0.05 deg if five measurements are made and averaged), provided the basal pole is more than 10 deg from the normal to the surface. Since the position of the basal plane trace in a grain can be determined by the sensitive tint technique to within 1 deg or better (again if the basal pole is tilted more than 10 to 15 deg from the normal of the surface), the location in space of the basal pole of a grain can be determined to within ±3 to 4 deg, but it is not then known on which side of the basal plane trace it lies. A tilting stage which will permit the specimen to be rotated 5 to 10 deg about the basal plane trace can be used to determine whether or not the angle of rotation increases or decreases with the tilt. This will then remove the ambiguity and the basal pole position can be located uniquely. Such a tilting stage is being built.

The technique discussed above will allow us to determine, within a few degrees of error, the angle between the basal poles of neighboring grains in polycrystalline zirconium alloys by a single-surface

examination. This, in turn, will help in trying to determine: (1) why hydrides precipitate in certain grain boundaries and do not in others that appear equally favorable and (2) just what is the crystallographic relationships between neighboring grains that show a subtexture different from the preferred orientation of the neighboring region.

Oxide Film Studies

J. C. Banter

Experiments have been completed on the effects of fast neutron irradiation on the rate of dissolution of anodic oxide films into the zirconium-base metal. Comparison of the reflection spectra for unirradiated control specimens and irradiated [10^{19} fast (> 1 Mev) neutrons/cm^2] anodized specimens after vacuum annealing at 600°C for 1 and 2 hr showed that the same decrease in film thickness had occurred in both types of specimens. Thus, the rate of dissolution was not affected by this dose of fast neutron irradiation.

The spectra of any given specimen before and after the dissolution did show differences other than those attributable to the decrease in film thickness. The intensity of reflection was much lower for those specimens that had been vacuum annealed to partially dissolve the oxide film. Such strong absorption indicates that the nature of the oxide film was changed by the partial dissolution. Attempts to dissolve the metal from the annealed specimens to produce windows for transmission measurements resulted in penetration of the oxide films by the bromine-ethyl acetate solution used and vigorous attack of the underlying zirconium. This led to the eventual destruction of the specimens if the attack was allowed to proceed. The penetration of the partially dissolved oxide films suggests that the strong optical absorption observed is a result of defects produced in the film of such a nature as to cause them to lose their integrity.

Further annealing experiments, as well as electrical conductivity measurements on the films before and after annealing, are in progress with the hope that they may lead to a better characterization of the nature of the defects.

Preparation of Single Crystals of Zirconium and Zirconium Alloys

J. C. Wilson

A single-crystal sphere, 9/16 in. in diameter, was made which is suitable for studies at high magnification of the optical anisotropy as a function of crystallographic plane and of wavelength. Spheres are easily and routinely produced by electrical-discharge machining. They are chemically polished to remove the disturbed surface layers. For optical studies, it is necessary to eliminate the micron-size etch pits produced by all of the numerous chemical and electropolishing techniques that we have tried. A new methanol-perchloric acid electropolishing solution,[7] used at 50 v at −70°C, has been found to eliminate satisfactorily the etch pits made by other polishing solutions. The technique does leave a few faint etch pits in two narrow regions near $(10\bar{1}0)$ poles. These are not objectionable in the optical study.

A number of 5/8-in.-diam single-crystal rods were grown from as-deposited crystal-bar zirconium by a single zone-melting pass. This material will be used for comparison with zone-refined single crystals in oxidation experiments. Although some loss of iron occurred, the concentration of other contaminants is unlikely to have changed appreciably. Physical defects normally present in as-deposited crystal bars prevent their use without consolidation by melting.

Electrical-Discharge Machining[8]

J. C. Wilson

Electrical-discharge machining has proved invaluable for preparing metallurgical specimens at ORNL. The design, construction, and operation of simple, inexpensive electrical-discharge machining units will be described. We will show the capabilities of these machines for such

---

[7]E. N. Hopkins and D. T. Peterson, "A Universal Electropolishing Method," paper presented at the 19th AEC Metallographic Group Meeting, April 20–22, 1965 at Oak Ridge National Laboratory, Oak Ridge, Tennessee (proceedings to be published as ORNL-TM-1161).

[8]Abstract of paper presented at the 19th AEC Metallographic Group Meeting, April 20–22, 1965 at Oak Ridge National Laboratory, Oak Ridge, Tennessee (proceedings to be published as ORNL-TM-1161).

operations as: (1) cutting single crystals to specific orientations with a minimum of deformation; (2) machining spherical, single crystal, oxidation specimens; and (3) cutting cylindrical and flat tensile bars.

Zone Refining of Zirconium

J. C. Wilson

We have been able to reduce the carbon and oxygen contamination in the zone-refined material by modifying the baking and operation of our zone refiner. The carbon monoxide partial pressure and the total operating pressure of the system were reduced by sequential baking, assuming that pyrolysis of the pump oil was a source of carbon monoxide, even though cracking fragments from the pump oil could not be detected with a residual gas analyzer. Carbon contamination during each zoning pass is now 2 ppm or less; earlier, as much as 10 ppm per pass had been observed. Oxygen contamination has now been reduced to the point that the oxygen concentration can be held below 20 ppm during 4 zone passes.

The reduced level of contamination by the vacuum system is now permitting a study of the effects of zoning speeds (our standard rate is 2 in./hr) on purification, structure, and crystal growth.

Zone-refined zirconium has been furnished to the Materials Compatibility Group, Metals and Ceramics Division, for use in their study of gettering methods for determining the oxygen content of liquid metal systems. A small amount of zone-refined titanium has also been supplied to another group for their use in the study of saline water corrosion of titanium alloys in the water desalination program.

Properties of High-Purity Zirconium

J. C. Wilson

Recrystallization

We have resumed an investigation of the effects of purity on the recrystallization of cold-worked (90% reduction by rolling) zone-refined zirconium. The microstructures at the start of recrystallization can be resolved after using a methanol-perchloric acid electropolishing

solution[7] to metallographically prepare the specimens. Preliminary experiments indicate that this solution can also be used for thinning such specimens for transmission electron microscopy.

Recrystallization started in less than 10 hr at 175°C, and was essentially complete after 100 hr at 175°C, producing an average grain diameter of about 10 μ. The recrystallization in such heavily cold-worked specimens apparently takes place by a nucleation and growth process rather than by the "in situ recrystallization" reported by McGreary and Lustman[9] in crystal-bar zirconium. In spite of the improved metallographic techniques, it has not yet been possible to measure quantitatively the percentage of recrystallized metal at each annealing time.

Even lower recrystallization temperatures are likely to be observed after more severe working or other kinds of deformation processing. The edges of the specimens are locally deformed by shearing (after rolling but before annealing) and, in the vicinity of the sheared edges, recrystallization is invariably observed to occur before it is readily detectable in the center of the specimens where the measurements are normally made.

Oxidation

As a first step in the determination of the dependence of the rate of diffusion of oxygen on crystallographic direction (using single-crystal spheres), we have made preliminary measurements of the dissolution rate at 580°C of anodized films (approximately 4000 A thick) on the $(10\bar{1}0)$ face of a single crystal of iodide zirconium. The specimens were mounted on an electron-beam heated "hot plate" in vacuum so that the interference color of the film could be observed continuously during dissolution. The film thickness was estimated by comparing the color observed with a set of standard colors prepared by anodizing in a 1% KOH solution[10] and assuming a film thickness of 27 A/v. The initial rate

---

[9] R. K. McGreary and B. Lustman, Trans. AIME 197, 284 (1953).

[10] R. D. Misch, Acta Met. 5, 179 (1957).

of dissolution, 30 A/min, agreed with the data of Misch,[10] but the dissolution rate measured in this manner decreased with time. Misch found the dissolution rate to be linear with time (up to 30 hr) at 450°C, but this time corresponds to a solution of less than 30 A of film under his conditions.

Our preliminary experiments have shown that the lighting, surface preparation, and viewing conditions affect the apparent color of the films. A special assembly has been built that will enable us to follow the dissolution rate of the oxide films visually on a single-crystal hemisphere of zirconium. This will permit the determination of the orientation dependence of dissolution rates more exactly than they are presently known[11] to serve as a guide for future experiments with flat single crystals.

[11]J. P. Pemsler, The Diffusion of Oxygen in Zirconium and Its Relation to Oxidation and Corrosion, NMI-1177 (1957).

[redacted]

5. CONTROLLED PRECIPITATION IN NUCLEAR CERAMICS

W. O. Harms

Practical limitations to the use of nuclear fuels for a variety of applications are associated with fission-gas release and irradiation-induced swelling due to the formation and migration of unstable fission-gas bubbles. More generally speaking, the useful application of nuclear ceramic materials — including nonfissile compounds used as structural components or dispersed-fuel diluents — is limited by poor resistance to thermal and mechanical shock. The behavior of these materials is very dependent upon microstructure, and it is through control of the latter that improvements must be sought.

Accordingly, a new program has been undertaken in the Fuels and Materials Development Program for FY-1966 to investigate means for preventing, or at least substantially reducing, the gas release and swelling effects in fuel compounds and to increase the toughness or "work-to-fracture" of ceramic materials in general through controlled precipitation. Some introductory remarks, background information, and preliminary results with regard to nonfissile ceramics are presented below.

Effect of Precipitation on the Properties of Nonfissile Ceramics

D. I. Matkin[1]

The effect of impurities in solution upon the flow stress of single crystals with the rock-salt structure (e.g., NaCl, MgO) is well known. Recently Groves and Fine[2] have studied precipitation hardening in iron-doped MgO that had been heat treated to precipitate magnesio ferrite ($MgO \cdot Fe_2O_3$). However, to increase the resistance to thermal and mechanical shock, it is necessary to either prevent the nucleation of cracks or to prevent the propagation of cracks through these materials.

---

[1]On loan from AERE, Harwell, England.

[2]G. W. Groves and M. E. Fine, J. Appl. Phys. 35, 3587 (1964).

[redacted]

Initial work on doped and heat-treated single crystals of NaCl (ref. 3) has indicated that a homogeneous distribution of voids and gold platelets (size approx 2 μ) act in the manner of "crack-stoppers." However, no studies have been made to determine the optimum shape and size of precipitates to give the maximum resistance to crack propagation.

Studies on MgO have shown that it is possible to control the state of precipitation of the impurities already present in nominally pure crystals. As-received crystals contain spherical or disk-shaped precipitates with diameters of 0.2 to 0.5 μ and, after suitable heat treatment, whisker-shaped precipitates of $CaO \cdot ZrO_2$ up to 100 μ long have been grown.[4]

In the present program the effect of whisker-shaped precipitates on crack propagation in Al_2O_3 is being investigated. Initial work has been to characterize single-crystal Al_2O_3 doped with TiO_2 that has been grown by flame fusion at the following laboratories: Crystal Products, Linde Division, UCC; G.E.C., Wembley, England; and Crystal Physics Group of Metals and Ceramics Division, ORNL. Measurement of the distribution of titanium throughout a crystal by Laser "microprobe" spectrographic analysis (Analytical Chemistry Division, ORNL) has indicated as much as a 50% variation in boules grown by flame fusion.

A standard Zeiss Ultraphot optical microscope has been modified for ultramicroscopy in order to study the distribution of precipitates and voids in polished, thin sections of a crystal. Figure 5.1 shows whisker-shaped precipitates observed by this technique in a thin basal section of a Linde commercial star ruby (Cr-doped Al_2O_3). Figure 5.2 shows the boundary between a region containing voids and a clear region in a thin prismatic section of a TiO_2-doped alumina boule, as revealed by ultramicroscopy.

---

[3]C. T. Forewood and A. J. Forty, to be published in Philosophical Magazine.

[4]D. I. Matkin and D. H. Bowen, Whisker Growth Within Single Crystals of Magnesium Oxide, AERE-R-4915 (April 1965).

The immediate aim is to produce, by suitable heat treatment, a homogeneous distribution of whisker-shaped precipitates in single crystal Al_2O_3, and then to assess the effect of these precipitates on crack propagation.

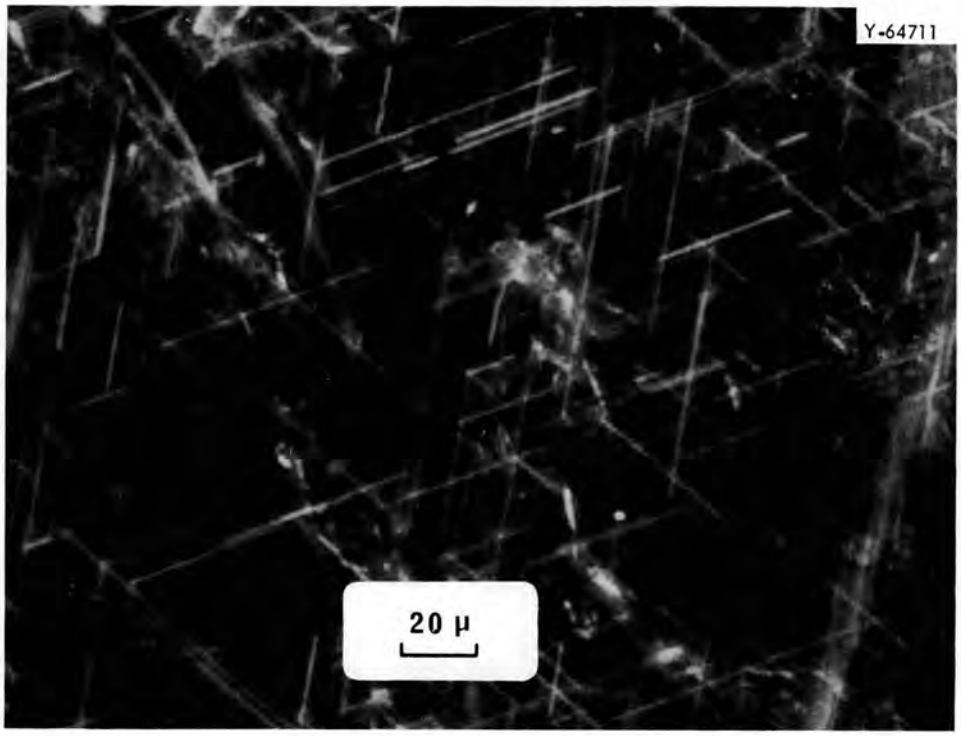

Fig. 5.1. Whisker-Shaped Precipitates in a Basal Section of Commercial Star Ruby, Revealed by Ultramicroscopy.

[redacted]

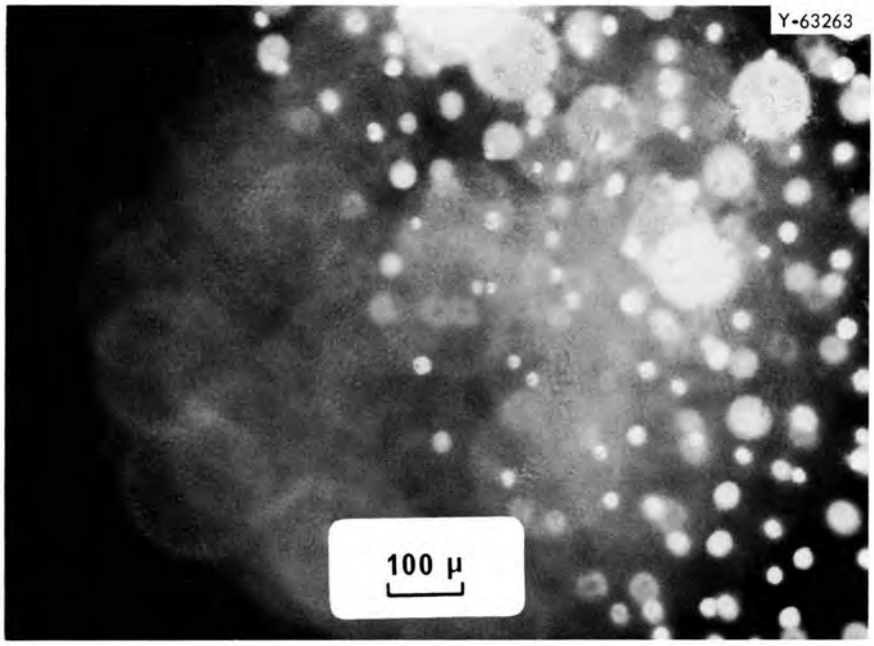

Fig. 5.2. Voids in a Prismatic Section of a TiO_2-Doped Al_2O_3 Boule, Revealed by Ultramicroscopy.

[redacted]

[redacted]

[redacted]

[redacted]

PART II

REACTOR CHEMISTRY DIVISION

[redacted]

[redacted]

[redacted]

[redacted]

6. FISSION-GAS RELEASE FROM FUEL MATERIALS DURING IRRADIATION

R. M. Carroll O. Sisman

This is the first reporting of a program that is newly sponsored by the Reactor Fuels and Materials Development Branch. The fission-gas release studies are not new, however, and we are therefore presenting a summary of the status of these studies.

About five years ago, we began construction of an experimental apparatus to be used in the Oak Ridge Research Reactor to determine the diffusion coefficients of xenon and krypton in fuel materials while they were producing power. Our immediate goal was to obtain engineering measurements to fit into a formula that would describe the fission-gas diffusion through uranium dioxide. However, as the experiment progressed it became apparent that classical diffusion processes did not control the fission-gas release. In trying to discover the factors that do control the fission-gas release, our experimental approach had gradually changed from engineering tests to basic properties studies.

We do not yet have a finished equation for calculating the fission-gas release from UO_2, but a defect-trap model has been formed which qualitatively describes the mechanism of fission-gas release. We will discuss the observations that led to the model, the experiments that have been made to test the model, and outline our current method of attack.

Experimental Method

Details of the in-reactor experimental apparatus and techniques for the fission-gas experiments have been reported.[1,2] Briefly, the UO_2 specimen is heated by its own fission power, which is regulated by moving the specimen into or out of the neutron flux of the Oak Ridge

[1]R. M. Carroll and C. D. Baumann, Experiment on Continuous Release of Fission Gas During Irradiation, ORNL-3050 (1961).

[2]R. M. Carroll, P. E. Reagan, Nucl. Sci. Eng. 21(2), 141–46 (1965).

[redacted]

Research Reactor (see Fig. 6.1). The specimen temperature is controlled by air cooling the capsule that contains the specimen. A continuous flow of sweep gas (97% He–3% H_2) carries the fission gas outside the reactor where it is analyzed by gamma-ray spectrometry. The hydrogen maintains the stoichiometry of the specimen.

ORNL-DWG 64-7278

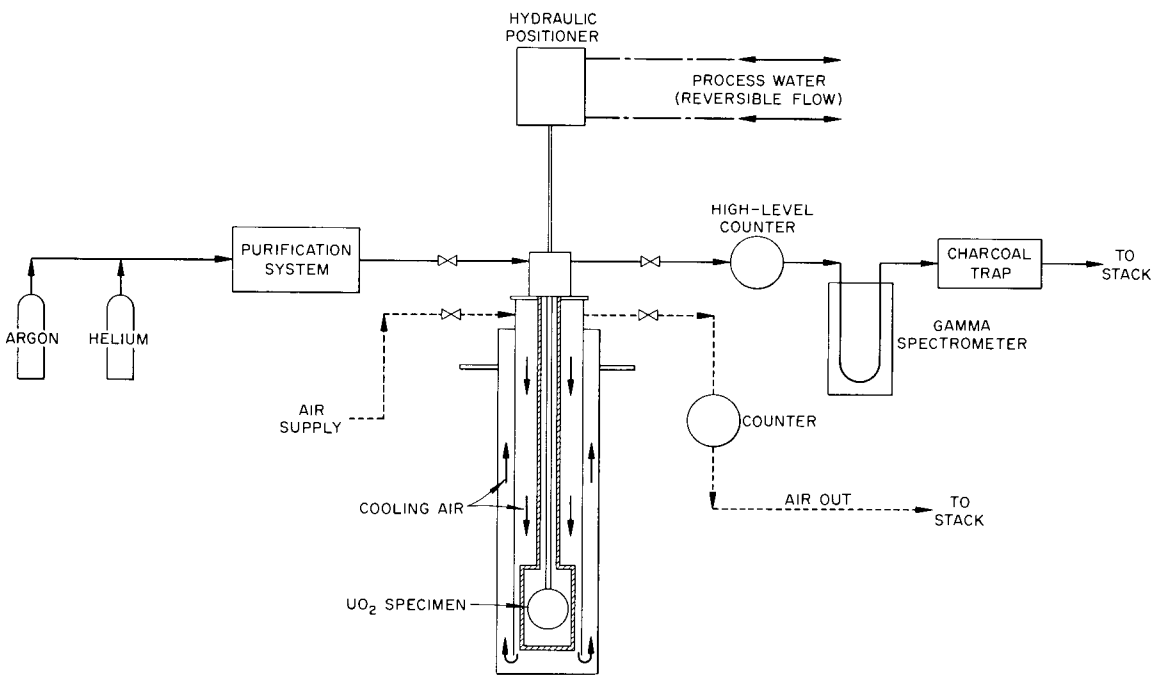

Fig. 6.1. Dynamic Fission-Gas Release Apparatus.

The neutron flux at the specimen is measured by using a sweep gas with a known argon concentration and measuring the neutron activation of the argon. (The argon peak may be recorded along with the fission-gas spectrum and is therefore a very simple measurement.)[3]

We select the UO_2 specimens with great care, since it has been well established that the physical properties of UO_2 (e.g., density, surface

[3]R. M. Carroll, Nucleonics 20(2), 42 (1962).

area, and oxygen-to-uranium ratio) have a very strong effect upon fission-gas release. In order to reduce the number of parameters affecting the gas release, all the specimens are of nearly theoretical density (10.96 g/cm^3), are of stoichiometric composition, contain no detectable porosity, and the total impurities are less than 200 ppm. The specimens are machined into thin disks 0.10-cm thick and 1.27 cm in diameter.

The experiment capsule is shown in Fig. 6.2. The highest temperature in the specimens is in the space between the two fuel disks. This temperature is measured by tungsten-rhenium thermocouples. Because the slabs are thin, the temperature drop across the specimen is small, and we can assign a definite temperature to a measured fission-gas release. Because of the small temperature drop, the specimens can be operated at power densities in excess of 130 w/cm^3 without danger of cracking from thermal stresses. The temperature is regulated over a wide range in order to determine the change in gas-release rate with change in temperature. The neutron flux is varied independent of temperature in order to determine the effect of fissioning rate.

The experiment is easily adapted to physical property measurements, and we have already made some crude measurements of thermal conductivity and somewhat better measurements of electrical conductivity in UO_2 during irradiation.[1,4]

---

[4]M. D. Karkhanavola and R. M. Carroll, In-Pile Measurement of the Electrical Resistivity and Thermoelectric Power of Sintered UO_2, ORNL-3093 (1961).

[redacted]

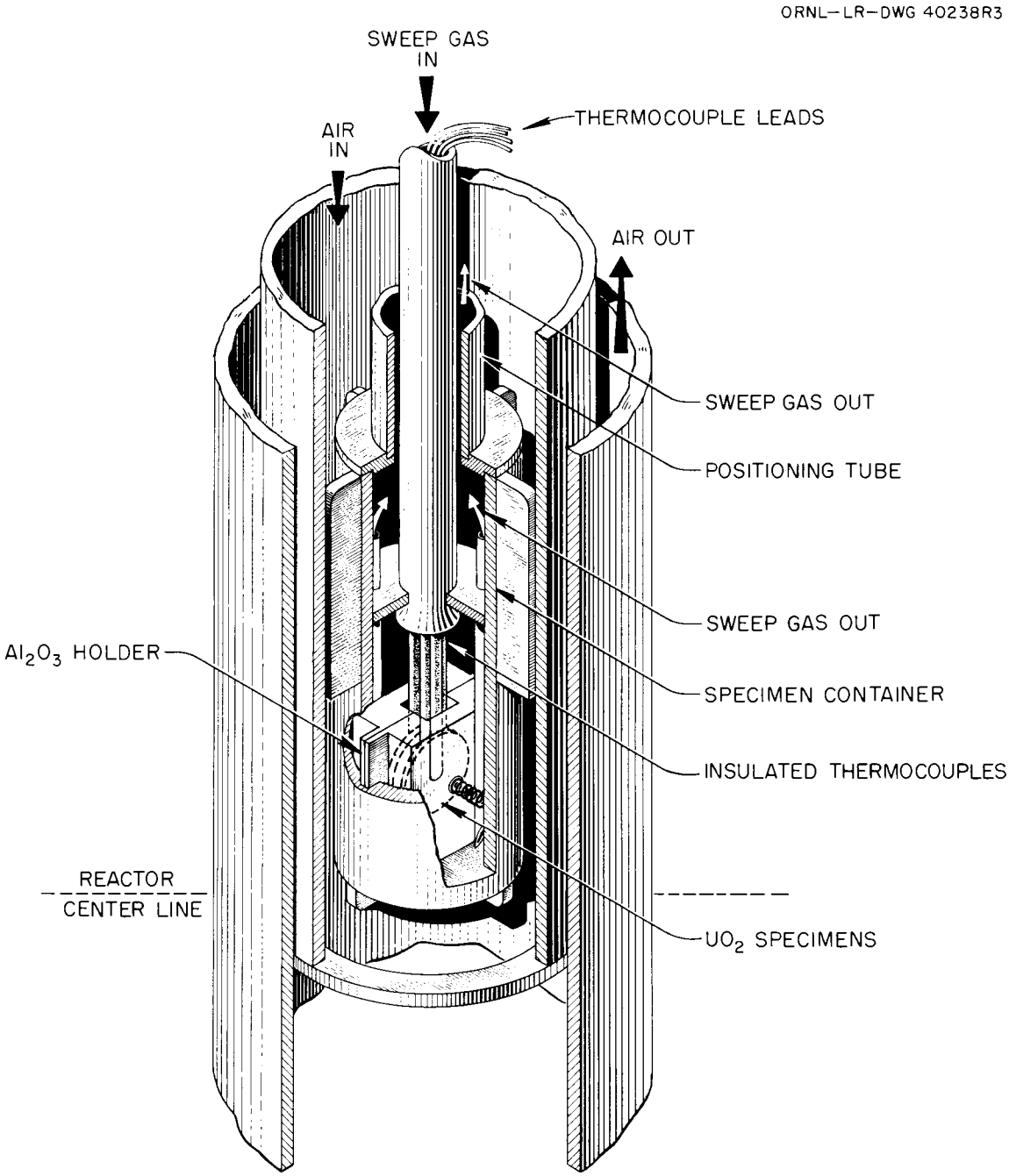

Fig. 6.2. Details of the Experimental Capsule.

[redacted]

Release of Fission Gas

Our experimental observations and the conclusions which have been drawn from them have been documented in a number of publications.[5–13] Some of the outstanding results which show that diffusion is not the controlling mechanism for fission gas in these experiments are discussed below and compared with results expected by diffusion theory. Many more arguments for the defect-trap model may be found in the references.

During irradiation, there are two basic processes by which fission gas is released from UO_2. The first process is independent of temperature and is proportional to fission rate. This process is responsible for the major portion of the gas release at temperatures below about 600°C. The amount of gas released by the second process increases exponentially with temperature and accounts for the major portion of the

---

[5]R. M. Carroll, "Continuous Release of Fission Gas from UO_2 During Irradiation," Symposium on Radiation Effects in Refractory Fuel Compounds, Am. Soc. Testing Mater. Spec. Tech. Publ. 306, 110–22 (1961).

[6]R. M. Carroll and O. Sisman, Nucl. Sci. Eng. 21(2), 147–58 (1965).

[7]R. M. Carroll, R. B. Perez, and O. Sisman, J. Am. Ceram. Soc. 48(2), 55–59 (1965).

[8]R. M. Carroll and O. Sisman, "In-Pile Fission-Gas Release from Fine-Grain UO_2," accepted for publication by the Journal of Nuclear Materials.

[9]R. M. Carroll, "Fission-Gas Release from UO_2 During Irradiation," Nucl. Safety 4(1) (1962).

[10]R. M. Carroll, "Fission-Product Release from UO_2," Nucl. Safety 5(4) (1964).

[11]R. M. Carroll, "Fission Product Release from Fuels," Nucl. Safety 6(4) (Summer 1965).

[12]R. M. Carroll and O. Sisman, "Fission-Gas Release During Fissioning in UO_2," Trans. Am. Nucl. Soc. 8(1), 22 (1965). To be published in Nuclear Applications.

[13]R. M. Carroll, "The Behavior of Fission-Gas in Fuels," paper to be presented at the AIME Conference on Radiation Effects in Materials, Asheville, N. C., September 8–10, 1965. To be published in proceedings.

gas release at temperatures above about 800°C. These two processes are illustrated in a plot of release rate vs temperature, Fig. 6.3. By traditional theory, these two processes would be described as recoil release (temperature independent) and diffusion release (temperature dependent).

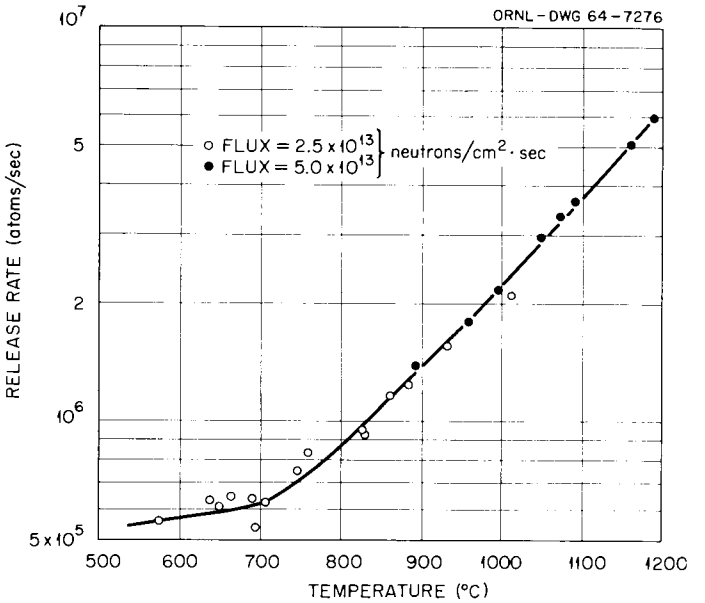

Fig. 6.3. Release Rate of ^{88}Kr from Fine Grain Specimen (C1–12) of UO_2.

Recoil Escape

During irradiation, fission gas will escape from the fuel structure by a recoil process, since when fission occurs within about 10 μ of the surface of UO_2 it is possible for a fission fragment to recoil free of the fuel. The amount of recoil escape can be easily calculated but such calculations are often misleading for the following reasons:

(1) The fission fragment usually leaves the UO_2 surface with sufficient energy to embed in solid surfaces near the specimen and thus will not be released.

(2) When the fission fragment leaves the UO_2 surface an average of about 2000 UO_2 molecules are ejected, and fission products in this knock-out zone are ejected along with the UO_2 (ref. 7).

We can determine if the fission gas is liberated by direct recoil or by knockout by comparing the relative amounts of different isotopes in the fission gas. This comparison shows that at UO_2 temperatures below 600°C most of the fission gas is emitted by the knockout process.[6]

The amount of gas liberated by knockout is directly proportional to the total (BET) surface area of the fuel whereas the amount of gas liberated by direct recoil is proportional to the geometric surface area. We find that the temperature-independent release, although directly proportional to the fission rate (see Fig. 6.4), is not proportional to the geometric surface. The total surface areas of the specimens as shown in Fig. 6.4 are quite different even though the geometric surface areas are the same.

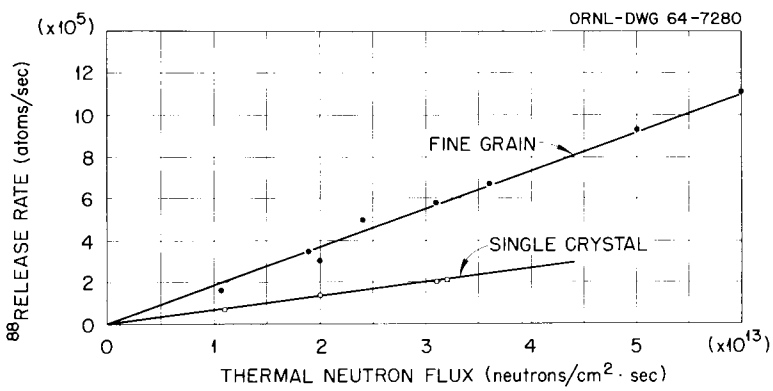

Fig. 6.4. Comparison of ^{88}Kr Recoil Release Between Single Crystal and Fine Grain UO_2 Specimens of the Same Size and Density.

Temperature-Dependent Release

The temperature-dependent component of the fission-gas release is obtained by subtracting the temperature-independent contribution from the total measured gas release. An Arrhenius plot of the temperature-dependent gas release is shown in Fig. 6.5. The fact that this plot yields a straight line has often been considered as confirmation that the fission-gas release was by a diffusion process. Actually, all processes governed by a factor $\exp\left(-\frac{\text{constant}}{\text{temperature}}\right)$ will have the same general form.

[redacted]

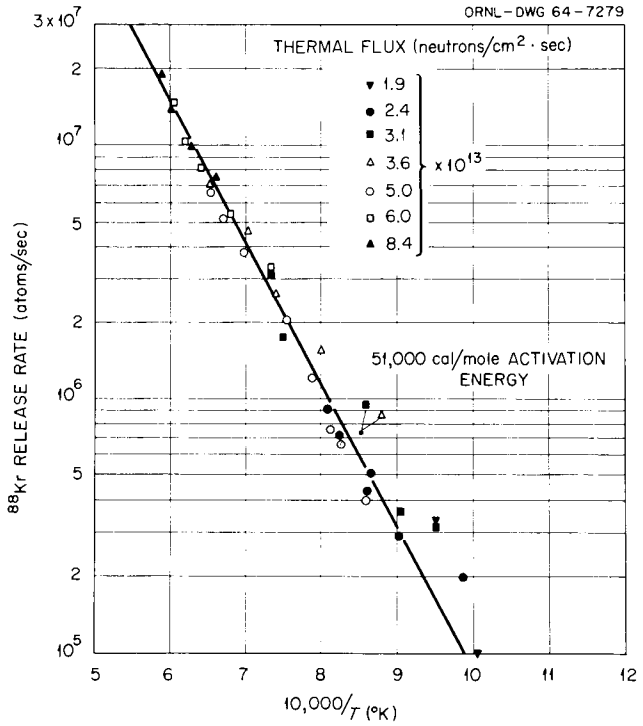

Fig. 6.5. Temperature-Dependent Release Rate of ^{88}Kr from Fine Grain UO_2.

It was first assumed that diffusion in UO_2 occurred by a vacancy process. To test this theory, specimens were irradiated at different fission rates but at a constant temperature. It was thought that the higher fission rates would accelerate diffusion because the fissioning process creates vacancies. Contrary to this theory, we found that a higher fission rate apparently retarded diffusion so that the diffusion coefficient appeared to decrease in direct ratio to the increase of fission rate.[6] What was actually being observed was a constant gas-release rate even though the rate of production of gas was increasing with increasing fissioning rate (see Figs. 6.3 and 6.5).

The results of Fig. 6.5 are directly opposite to that expected for the diffusion of atoms through a matrix. Regardless of the mechanism by which diffusion occurs, the release should be proportional to the concentration of the gas in the specimen. The data in Fig. 6.5 show that the concentration of ^{88}Kr within the specimen was changed by more than a factor of 4 without producing a significant change in the release

[redacted]

rate. We have explained this result by postulating that the fission-gas release is controlled by a trapping mechanism rather than a diffusion process and on the basis of this postulate the defect-trap model was formed.

Defect-Trap Model

The experiments with single crystal UO_2 led to the formulation of the defect-trap model for fission-gas release during irradiation.[6] In this model we assume that the rate-controlling process for fission-gas release in the temperature-dependent region (above approx 600°C for UO_2) is the probability of the gas being trapped and the probability of being released from traps. The traps are divided into three categories:

1. intrinsic traps, which are voids, grain boundaries, or other flaws in the material;
2. point defects, which are formed in the wake of a fission fragment; and
3. clusters of point defects.

The second and third types of defects are formed by irradiation, while the first is an inherent property of the material (see Fig. 6.6).

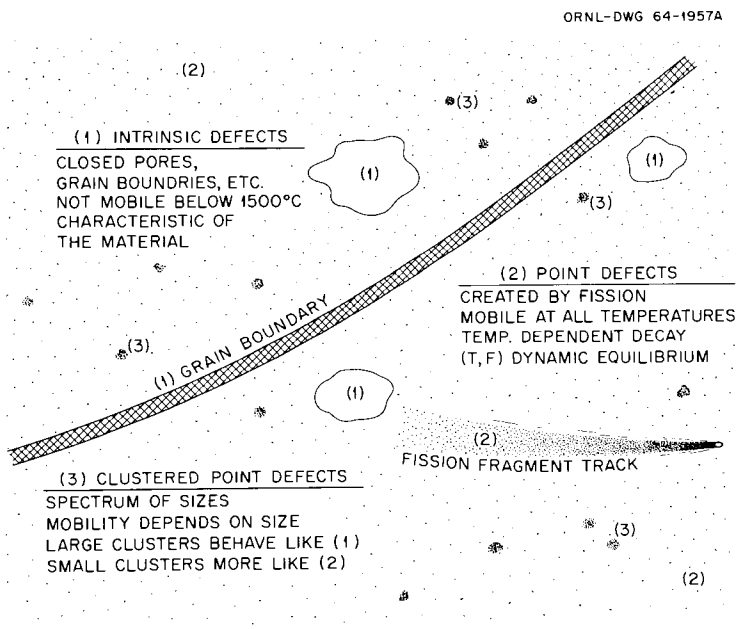

Fig. 6.6. Defect-Trap Characteristics.

Theoretical Considerations

For the defect-trap theory, we propose that when a diffusing fission-product atom encounters a point defect it is trapped there, but that it has a probability of escape from the trap which increases with temperature. Also, an energetic fission fragment passing nearby will free the fission product from the point defect trap. If the point defect does not either trap a fission product or combine with a cluster of point defects, it will soon anneal and vanish. The time required for annealing is also a function of temperature. Consequently, the population of point defects will reach a production-decay equilibrium.

By the defect-trap theory, the fission gas would diffuse rapidly through the UO_2 matrix and the escape rate from the specimen would be controlled by the probability of not being trapped in a defect. The proportion of fission gas which escapes from the specimen is small (less than 10^{-3} at temperatures below 1300°C), indicating that the probability of fission products being trapped is large and that only gas near the surface of the specimen will escape.

The trapping probability decreases as the temperature increases because the annealing rate of the point defects increases with temperature. Also, the probability of escape for a fission product trapped in a point defect (or a cluster of point defects) would increase with temperature. The probability of a trapped fission product escaping from the defect would vary with the size of the defect; the intrinsic flaw presents a deep trap from which there is small probability of escape. The intrinsic flaws are large enough so that diffusion of the flaw (at temperature not exceeding 1500°C) would be negligible.

Once having established a production-decay equilibrium of point defects, it follows that the population density of defects will increase in proportion to the increase in fission rate (at least until the fission rate is so great that the fission tracks are eliminating a significant portion of the existing point defects). Consequently, the trapping probability would increase with fission rate and this would produce a lower fractional escape rate of gas (release rate per production rate).

Grain Boundary Effect

By the diffusion model for fission-gas release, a grain boundary is assumed to provide an avenue of rapid diffusion. On the other hand, the defect-trap model postulates that grain boundaries will anchor migrating fission gas. Therefore, a good test of one aspect of the defect-trap model is to compare fission gas released for specimens of different grain size. To do this we have made in-reactor tests comparing the release of fission gas from single crystals of UO_2 to that from fine grain UO_2 (ref. 14). Both type specimens were cut and ground to the same size and surface finish. The density, chemical composition, and irradiation conditions of both types of specimens were almost identical. The essential differences between the specimens was that one had many grain boundaries (grain size was approx 3 μ) and the other had none.

The ^{88}Kr release from the fine-grain specimens was found to be 17 times lower (at 1000°C) than for the single crystals (see Fig. 6.7). Metallographic examination showed a broadening of the grain boundaries for the irradiated fine-grain specimen (2.5×10^{19} fissions/cm^3 burnup) indicating a trapping of fission products at the grain boundaries. These observations support the defect-trap theory and indicate that grain boundaries in UO_2 act as traps rather than avenues of rapid escape.

As with single-crystal specimens, the temperature-dependent fission-gas release from the fine-grain specimens did not change significantly with fission rate (see Fig. 6.7). The results from the fine-grain specimens were confirmation of the defect-trap model, which indicated that the magnitude of the fission-gas release would be influenced by intrinsic traps but that the change of release rate with fission rate would be controlled by point defects. The data of Fig. 6.5 have a temperature range of 700 to 1450°C and a fission density range of 2 to 9×10^{12} fissions cm^{-3} sec^{-1}.

---

[14]R. M. Carroll, "Fission-Gas Release from UO_2 Irradiation," Nucl. Safety 4(1) (1962).

[redacted]

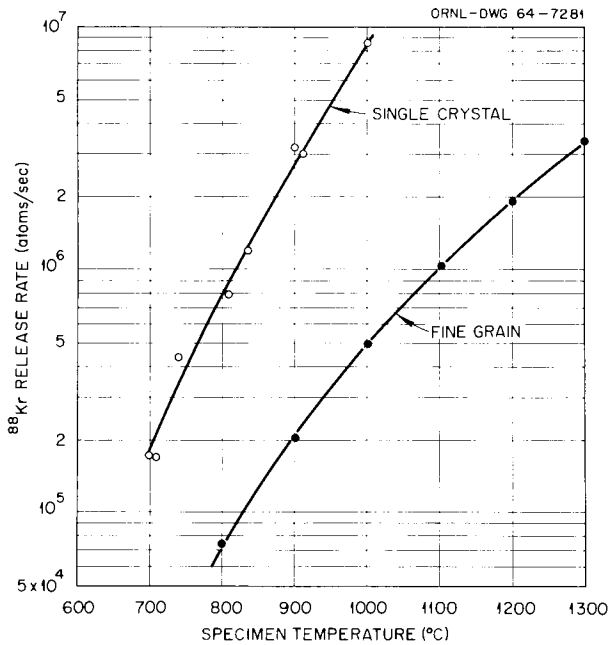

Fig. 6.7. Temperature Dependent ^{88}Kr Release Rate Normalized to Single Crystal Surface Area.

Dynamic Experiments

A mathematical expression has been derived for mother-daughter release of fission gas, based on the defect-trap theory described. The derivation of the mathematical model and some tests as to its validity are discussed elsewhere.[15,16] Qualitatively the model appears to satisfy all of the experimental observations.

There are, however, too many variables to be evaluated by the steady-state experiments. By operating the experiments in a dynamic mode we can gain the extra degree of freedom necessary to make this evaluation.

The experimental facility has now been altered so that one experimental parameter can have a slight ripple imposed about a selected steady-state level. The principle of this method is that different

---

[15]R. M. Carroll, R. B. Perez, and O. Sisman, J. Am. Ceram. Soc. 48(2), 55–59 (1965).

[16]R. B. Perez, "A Dynamic Method for In-Pile Fission-Gas Release Studies," Trans. Am. Nucl. Soc. 8(1), 22–23 (1965). To be published in Nuclear Applications.

[redacted]

functions will have a different rate of response (in effect a sort of inertia) to a change in conditions. We expect that data from the dynamic experiments along with data from the steady-state experiments will allow us to fully evaluate the constants in the equation for the defect-trap model.

Experimental Method

Extensive modifications of the experiment controls were required to allow a precise oscillation about a selected steady-state condition. The fission rate is oscillated by moving the specimen in and out of the neutron flux. We can program the flux level and the amplitude, frequency, and wave shape of the flux oscillation. The neutron flux does not vary lineally with distance and we had expected that an eccentric motion of the specimen would be necessary to obtain a sinusoidal oscillation of flux. However, because the movement of the specimen is very slight, the change of flux is proportional to the movement and a sinusoidal oscillation of the specimen produces a sinusoidal oscillation of neutron flux. By using a sweep gas containing 1% Ar and continuously measuring the neutron activation of the argon,[17] we determine the wave shape of the flux oscillation.

The specimen temperature is oscillated by a controlled cooling air flow over the specimen capsule (see Fig. 6.1). The specimen temperature is measured by thermocouples which are connected into a feedback system to automatically control the air cooling to produce a desired temperature. Thus, the temperature can be programmed to oscillate about a given value with a selected amplitude, frequency, and wave shape.

The fission-gas release from the specimen during oscillations is measured by continuous gamma-ray analysis of the flowing sweep gas. The gamma-ray spectrometer is programmed to measure the time-dependent variation of a given isotope of the fission gas (usually ^{88}Kr). The delay time required for the fission gas to flow out of the reactor is

---

[17] R. M. Carroll, Nucleonics 20(2), 42 (1962).

determined by using sweep gas that contains argon and measuring the time lapse between position oscillations and argon activity oscillations. A precise record of time-temperature or time-flux is kept with a digital recording clock-voltmeter. The fission-gas release rate measurements are thus synchronized with the temperature or flux oscillations of the specimen.

No quantitative conclusions have been obtained as yet from the oscillating experiments but this method appears very promising. The qualitative results of the oscillating experiments support the defect-trap model. The preliminary curves from the oscillating experiments are proving very interesting. These results will be presented in the next quarterly report along with some of the mathematical analyses of both the oscillating and steady-state experiments.

[redacted]

7. PHYSICAL PROPERTIES OF FUEL MATERIALS DURING IRRADIATION

M. F. Osborne O. Sisman

The effect of radiation on the physical properties of many refractory fuel materials has been studied extensively. Most of these measurements, however, have been performed after irradiation. The fission process itself and the presence of highly ionized fission fragments and other atoms which have been displaced by fission neutrons, cause large, short-lived distortions in the crystal structure of the fuel material. Therefore, it seems quite likely that such properties as thermal conductivity, electrical conductivity, specific heat, coefficient of thermal expansion, and modulus of elasticity for a material which is actively undergoing fission may be significantly different from such properties in the same material after fissioning has stopped. Indeed, studies of fission-gas release both during and after irradiation have demonstrated the likelihood of differences during irradiation. Consequently, we plan to measure the pertinent properties of a variety of fuel materials while they are being maintained at realistic temperatures and fission rates.

Since thermal conductivity is generally considered to be the most important of these properties and UO_2 is one of the most widely used fuel materials, the thermal conductivity and the specific heat of a cylindrical single crystal of UO_2 will be studied in our first experiment. One of the Oak Ridge Reactor core facilities and the instrumentation developed for the fission-gas release studies will be utilized. The experimental configuration will be modified to include auxiliary electrical heat. The fuel specimen is a UO_2 single crystal 0.235 in. in diameter and 1.94 in. long; a 0.063-in.-diam center hole is 1.10 in. deep. The temperatures at the center and at the outside surface of the specimen will be monitored by thermocouples. The neutron flux, and hence the heat generation rate, will be controlled by adjusting the position of the specimen within the reactor and will be measured by adding argon to the helium sweep gas and determining the extent of argon activation. The specimen temperature will be controlled by

[redacted]

regulation of the cooling air flow around the capsule and of the electrical heat input within the capsule. Thus, the heat generation rate and the temperature of the specimen may be varied independently.

After steady-state measurements of the thermal conductivity have been obtained over a wide range of temperatures and heat generation rates, the dynamic techniques developed and used in fission-gas release studies will be applied. Through the reduction of data obtained during transient conditions, we hope to minimize any inaccuracies in temperature measurement. By repeating the measurements at regular intervals during an extended irradiation period, the effect of uranium burnup and the accumulation of lattice defects within the crystal will be investigated.

In subsequent experiments we will investigate electrical conductivity and the effects of higher fuel burnup through the use of enriched uranium, and the study will be extended to other fuel materials, such as ThO_2-UO_2, BeO-UO_2, and PuO_2. Studies of the thermal expansion and elastic constants will require considerable modification of the experimental techniques, and so must be approached later in the program.

[redacted]

Previous reports in this series are:

ORNL-TM-920	Period Ending June 30, 1964
ORNL-TM-960	Period Ending September 30, 1964
ORNL-TM-1000	Period Ending December 31, 1964
ORNL-TM-1100	Period Ending March 31, 1965

[redacted]

[redacted]

[redacted]

[redacted]

Internal Distribution

1-3. Central Research Library
4-5. ORNL - Y-12 Technical Library
Document Reference Section
6-15. Laboratory Records
16. Laboratory Records, RC
17. ORNL Patent Office
18. G. M. Adamson, Jr.
19. J. C. Banter
20. J. H. Barrett
21. S. E. Beall
22. M. Bender
23. R. G. Berggren
24. J. O. Betterton, Jr.
25. D. S. Billington
26. A. L. Boch
27. B. S. Borie
28. G. E. Boyd
29. W. H. Bridges
30. R. B. Briggs
31. W. E. Brundage
32. R. M. Carroll
33. J. V. Cathcart
34. G. W. Clark
35. K. V. Cook
36. J. H. Crawford
37. J. E. Cunningham
38. J. H. DeVan
39. C. V. Dodd
40. D. A. Douglas, Jr.
41. J. I. Federer
42. B. E. Foster
43. A. P. Fraas
44. J. H Frye, Jr.
45. R. J. Gray
46. W. R. Grimes
47. J. P. Hammond
48. W. O. Harms
49. R. L. Heestand
50. M. R. Hill
51. N. E. Hinkle
52. H. W. Hoffman
53. H. Inouye
54. T. N. Jones
55. G. W. Keilholtz
56. B. C. Kelley
57. J. A. Lane
58. C. F. Leitten, Jr.
59. A. L. Lotts
60. R. N. Lyon
61. H. G. MacPherson
62. R. E. MacPherson
63. M. M. Martin
64. W. R. Martin
65. R. W. McClung
66. H. E. McCoy, Jr.
67. H. C. McCurdy
68. R. E. McDonald
69. D. L. McElroy
70. C. J. McHargue
71. F. R. McQuilkin
72. A. J. Miller
73. E. C. Miller
74. F. H. Neill
75. S. M. Ohr
76. M. F. Osborne
77. P. Patriarca
78. F. H. Patterson
79. A. M. Perry
80. S. Peterson
81. M. L. Picklesimer
82. P. L. Rittenhouse
83. W. C. Robinson
84. M. W. Rosenthal
85. G. Samuels
86. H. W. Savage
87. J. L. Scott
88. O. Sisman
89. G. M. Slaughter
90. G. P. Smith, Jr.
91. S. D. Snyder
92. I. Spiewak
93. J. T. Stanley
94. W. J. Stelzman
95. J. O. Stiegler
96. A. Taboada
97. D. B. Trauger
98. G. M. Watson
99. M. S. Wechsler
100. A. M. Weinberg
101. J. R. Weir, Jr.

[redacted]

[redacted]

102. W. J. Werner
103. G. D. Whitman
104. J. M. Williams
105. R. O. Williams
106. J. C. Wilson
107. H. L. Yakel, Jr.
108. F. W. Young, Jr.
109. C. S. Yust

External Distribution

110–112. F. W. Albaugh, GE, Hanford
113. A. J. Alexander, AEC, CANEL
114. R. J. Allio, Westinghouse Atomic Power Division
115. R. D. Baker, Los Alamos Scientific Laboratory
116. L. Brewer, University of California, Berkeley
117. V. P. Calkins, GE, NMPO
118. W. Cashin, Knolls Atomic Power Laboratory
119. S. Christopher, Combustion Engineering, Inc.
120. R. M. Cilimberg, Division of Reactor Development, AEC, Washington
121–122. D. F. Cope, AEC, Oak Ridge Operations
123. G. K. Dicker, Division of Reactor Development, AEC, Washington
124. E. A. Evans, GE, Vallecitos
125. W. C. Francis, Phillips Petroleum Company
126. R. G. Grove, Mound Laboratory
127. D. H. Gurinsky, BNL
128. S. Hasko, NBS
129. A. N. Holden, GE, APED
130. J. S. Kane, University of California, Livermore
131. J. H. Kittel, ANL
132. E. J. Kreih, Westinghouse, Bettis Atomic Power Laboratory
133. W. L. Larsen, Iowa State University, Ames Laboratory
134. J. H. MacMillan, Babcock and Wilcox Company
135. R. E. Pahler, Division of Reactor Development, AEC, Washington
136. S. Paprocki, BMI
137. D. Ragone, GA
138. L. M. Raring, Pratt & Whitney, CANEL
139. Division of Research and Development, AEC, ORO
140. A. H. Roberson, U. S. Department of the Interior, Bureau of Mines
141. W. Rostokev, Illinois Institute of Technology Research Institute
142. F. C. Schwenk, Division of Reactor Development, AEC, Washington
143–144. J. M. Simmons, Division of Reactor Development, AEC, Washington
145. L. E. Steele, Naval Research Laboratory
146. R. H. Steele, Division of Reactor Development, AEC, Washington
147. W. F. Sheely, Division of Research, AEC, Washington
148. A. Strasser, United Nuclear Corporation

[redacted]

[redacted]

149. W. R. Voigt, Division of Reactor Development, AEC, Washington
150. C. E. Weber, Atomics International
151. G. W. Wensch, Division of Reactor Development, AEC, Washington
152. M. J. Whitman, Division of Reactor Development, AEC, Washington
153-167. Division of Technical Information Extension

[redacted]